



# An injectable antibacterial wet-adhesive for meniscal cartilage regeneration via immune homeostasis mediated by SMSC-derived extracellular vesicles

Moran Huang<sup>a,1</sup>, Zhengchao Yuan<sup>b,1</sup>, Guojian Fu<sup>a,1</sup>, Jize Dong<sup>a</sup>, Yaying Sun<sup>a</sup>, Wenxin Wang<sup>b</sup>, Muhammad Shafiq<sup>c</sup>, Huiliang Cao<sup>d</sup>, Xiumei Mo<sup>b,\*\*</sup>, Jiwu Chen<sup>a,\*</sup>

<sup>a</sup> Department of Sports Medicine, Shanghai General Hospital, Shanghai Jiao Tong University School of Medicine, Shanghai, 200080, China

<sup>b</sup> State Key Laboratory for Modification of Chemical Fibers and Polymer Materials, Shanghai Engineering Research Center of Nano-Biomaterials and Regenerative Medicine, College of Biological Science and Medical Engineering, Donghua University, Shanghai, 201620, China

<sup>c</sup> Innovation Center of NanoMedicine (iCONM), Kawasaki Institute of Industrial Promotion, Kawasaki-ku, Kawasaki, 210-0821, Japan

<sup>d</sup> Interfacial Electrochemistry and Biomaterials, School of Materials Science and Engineering, East China University of Science & Technology, Shanghai, 200237, China

## ARTICLE INFO

Handling Editor: Dr Hao Wang

### Keywords:

Meniscus repair  
Cartilage regeneration  
Wet-adhesive hydrogel  
Extracellular vesicles  
Macrophage

## ABSTRACT

Surgical repair is recommended for meniscus tear to avoid knee degeneration. However, postoperative meniscal healing remains challenging due to limited blood supply, particularly the avascular zone. Tissue-engineering techniques had limited outcomes in meniscus repair due to the highly irregular interface of meniscus and the wet joint environment. Additionally, it was proved that the inflammation status and the recruitment of endogenous cells are crucial for meniscal healing. This study represents a versatile extracellular vesicles (EVs)-based wet-adhesive employed in meniscus repair. A novel injectable hydrogel adhesive, designated as oxidized dextran/carboxymethyl chitosan/poly-L-lysine/synovial mesenchymal stem cell-derived EVs (OD/CS-PL@EVs), was fabricated and demonstrated effective antibacterial activity against *S. aureus* and *E. coli*. This adhesive also exhibited effective adhesion to the waterish meniscus with a lap shear strength of 134 KPa. Additionally, it promoted the proliferation, migration, chondrogenic differentiation, and extracellular matrix formation of SMSCs and meniscus cells and induced the polarization of macrophages towards the M2 phenotype *in vitro*. The RNA sequencing results further proved that four inflammation-related signaling pathways were inhibited by the prepared products. After being administered into the rabbit meniscal defect model, OD/CS-PL@EVs hydrogel adhesive effectively regulated the inflammatory balance and facilitated the meniscal cartilage regeneration in the avascular area, further remarkably delaying the progression of osteoarthritis. In summary, OD/CS-PL@EVs hydrogel adhesive provided a promising strategy to promote meniscal repair in avascular zone repair of meniscus for future clinical applications, holding great potential in preventing osteoarthritis.

## 1. Introduction

The menisci could protect the knee joint through shock absorption, load distribution and stability maintenance [1]. After the menisci tear, it is important to preserve the menisci integrity for preventing knee degeneration [2]. As a heterogeneous fibrocartilage of avascular and low-cell-count structure, the torn menisci have the limited capability for regeneration and healing [3]. Clinical treatments mostly include arthroscopic partial meniscectomy (APM) and meniscal suture repair

techniques. APM is simple and widely utilized, but only brings about short-term clinical functional improvements. Frequently, APM sacrifices the intact meniscal cartilage structure, thereby hastening the progression of tissue degeneration and osteoarthritis [4]. In contrast, meniscal suture techniques (inside-out, outside-in and all-inside) are more in line with the goal of preserving the meniscal structure as much as possible [2]. However, meniscal suture techniques face challenges because the healing capacity of stitched tissues is limited, leading to a high rate of healing failure [5]. In addition, meniscal replacement surgery also

\* Corresponding author.

\*\* Corresponding author.

E-mail addresses: [huangmoran44@126.com](mailto:huangmoran44@126.com) (M. Huang), [yuanzhengchao2021@163.com](mailto:yuanzhengchao2021@163.com) (Z. Yuan), [fuwany2008@163.com](mailto:fuwany2008@163.com) (G. Fu), [djz9975@163.com](mailto:djz9975@163.com) (J. Dong), [yaying.sun@shgh.cn](mailto:yaying.sun@shgh.cn) (Y. Sun), [wangwenxin@mail.dhu.edu.cn](mailto:wangwenxin@mail.dhu.edu.cn) (W. Wang), [shafiqdr786@yahoo.com](mailto:shafiqdr786@yahoo.com) (M. Shafiq), [huiliang.cao@ecust.edu.cn](mailto:huiliang.cao@ecust.edu.cn) (H. Cao), [xmm@dhu.edu.cn](mailto:xmm@dhu.edu.cn) (X. Mo), [jeevechen@gmail.com](mailto:jeevechen@gmail.com) (J. Chen).

<sup>1</sup> These authors contributed equally.

<https://doi.org/10.1016/j.compositesb.2024.111970>

Received 29 May 2024; Received in revised form 6 November 2024; Accepted 11 November 2024

Available online 12 November 2024

1359-8368/© 2024 Published by Elsevier Ltd.

provides a solution for treating meniscal injuries. Commercially available collagen meniscal implant (CMI) has been used for partial meniscal replacement; however, newly formed tissue was reported to have biomechanical properties inferior to natural meniscal tissue. Moreover, meniscal allograft transplantation (MAT) has also been reported in clinical practice for partial or total replacement. However, MAT faces drawbacks such as a lack of suitable donors, storage challenges, and potential transmission of diseases [6]. Therefore, there is an urgent need to develop new treatment strategies to achieve effective management of meniscal injuries.

Various studies emphasized improving the re-integration of the torn meniscus in the avascular zone [3]. Although Hydrogel-based tissue engineering was widely used for improving the cartilage and meniscus healing at the interface [7–9]. Chen et al. constructed a GelMA-aptamer system with high specificity and affiliation to recruit both synovial and meniscal cells, this system effectively promoted meniscus regeneration for meniscal avascular area repair. In addition, Zhong et al. prepared injectable decellularized meniscus extracellular matrix (mECM) hydrogels for the purpose of in situ delivery of stem cells for the treatment of meniscus injuries, and the results demonstrated the hydrogels enhanced meniscus regeneration [10]. It was still ineffective for the torn meniscus because of the highly irregular interface, which might be resolved by the hydrogel adhesives [11,12]. Although commercial tissue adhesives have already been applied in numerous fields, such as hemostasis and skin wound repair, there is currently no specific tissue adhesive available for meniscal injury in clinical practice [13]. Recently, some researchers have seen transformative advances in achieving strong hydrogel adhesion [14,15]. A unifying principle to obtain strong hydrogel adhesion is achieved through the synergy of chemistry, topology, and mechanics. Specially, the primary polymer network in the hydrogel must connect to the other material through covalent bonds, noncovalent complexes, polymer chains, polymer networks, nanoparticles, etc [16]. Few attempts at using adhesives for meniscus repair might also suffer from drawbacks such as the need for improved biocompatibility and mechanical performance [17,18]. The copolymer adhesive was reported to be used in meniscus repair experiments. Although the elastic modulus is close to that of the natural meniscus, challenges related to biocompatibility persist [18]. Moreover, amphiphilic copolymer adhesive was used to repair meniscus torn due to superior adhesive strength, however, the adhesive takes too long to cure completely [19]. Up to now, only fibrin-based hydrogel adhesives were applied for clinical studies related to human meniscal repair, and the use of such exogenous clots was more likely to exploit the bioeffects of the contained platelet and serve as the scaffold rather than the adhesive [17]. In addition, the adhesion effect of the conventional hydrogel adhesives would reduce or even loss in the wet intra-articular microenvironment [20].

Recently, the wet-adhesive hydrogel was developed to effectively adhere to waterish tissues with various methods, including isocyanate bonds, N-hydroxy succinimide (NHS)-activated ester bonds, and Schiff base bond, and others [20]. The Schiff base bond, one of the methods of covalently binding to wet tissue, has been widely adopted and applied in the intra-articular wet environment [20,21]. As biodegradable and biocompatible polysaccharides, both dextran and carboxymethyl chitosan have obtained approval from the Food and Drug Administration (FDA) for a variety of biomedical applications [22]. A wet-adhesive hydrogel could be developed through a Schiff base reaction to generate a cross-linked structure based on the aldehyde groups of oxidized dextran (OD) and the amino groups of carboxymethyl chitosan (CS), forming a dual-component OD/CS hydrogel [23]. This hydrogel has a controllable network structure with high biocompatibility, which are expected to achieve effective adhesion to the meniscus. Furthermore, the adhesive strength and tissue adhesion characteristics could be regulated by adjusting the proportion of the two components [24].

Notably, an optimal tissue engineering scaffold, serving as an exogenous implant, is required to exhibit robust antibacterial capabilities. This ensures a secure environment for cells or bioactive tissues,

mitigating the risk of implant-related infections [25]. Unlike traditional antibacterial metal ions that might have cytotoxic effects, Poly-L-lysine (PL), a natural antibacterial peptide, has been FDA-approved and is extensively utilized in the treatment of infectious diseases owing to its biocompatibility and broad-spectrum antibacterial capabilities [26]. In addition, PL possesses abundant lysine residues that could replace hydrated cations on wet tissue surfaces and provide additional amino groups, thereby further enhancing wet adhesion [27]. Therefore, introducing PL into OD/CS hydrogel is expected to further enhance the hydrogel's cross-linking degree, reinforce the mechanical properties, and prepare high wet adhesive hydrogels with superior antibacterial properties.

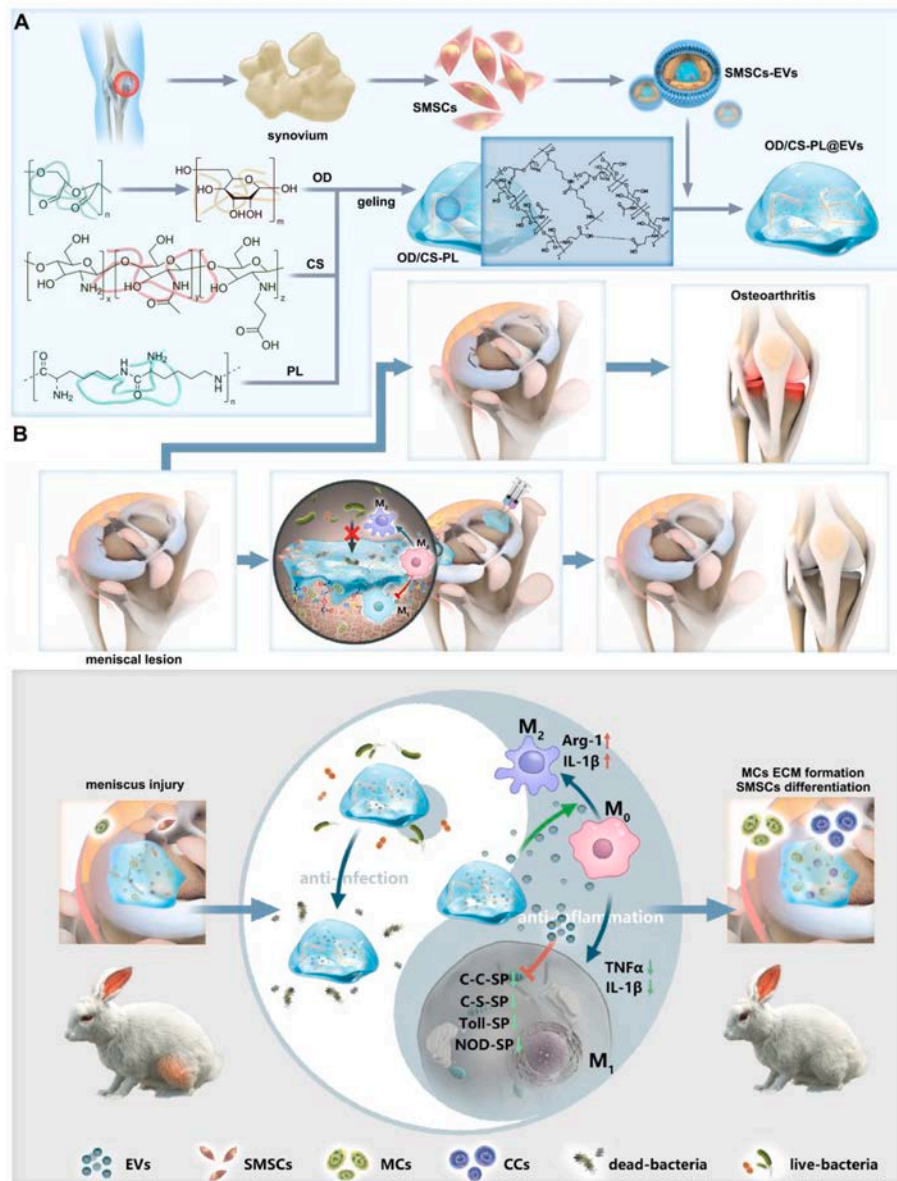
Current studies indicate that the endogenous cells promoting meniscal healing primarily originate from the synovium tissues and meniscus [9]. Within them, synovium-derived mesenchymal stem cells (SMSCs) and meniscus cells (MCs) are considered to play crucial roles in meniscal regeneration [28]. Therefore, achieving the proliferation and recruitment of endogenous SMSCs and MCs at the injury site may offer a promising approach for avascular meniscus repair. Up to now, stem cell transplantation has been applied as a treatment for meniscus injuries [29]. However, their application might pose potential risks such as tumorigenicity, immune rejection, and ethical concerns associated with direct stem cell transplantation [30]. In recent years, extracellular vesicles (EVs) derived from stem cells have garnered considerable attention due to their recognized biological functionalities, akin to those of stem cells [30]. As mentioned before, SMSCs are considered to exert a critical influence on the meniscal healing. The EVs derived from SMSCs have been reported to contribute to meniscus repair by fostering the proliferation and migration of endogenous cells, which also facilitate the chondrogenic differentiation of stem cells [31,32]. In addition, appropriate intervention in the inflammatory microenvironment state to promote tissue repair has become a crucial aspect in the realm of regenerative medicine [33,34]. Similarly, the immune microenvironment is in a pro-inflammatory state following meniscal injury, inevitably hindering effective meniscal regeneration [3,35]. By modulating the immune microenvironment, the goal of promoting meniscal regeneration might be achieved [34,36]. Moreover, the stem cell-derived EVs were reported to have excellent performance in inflammation regulation and guidance of stem cell behavior [37]. We speculated that SMSCs-EVs could provide tremendous assistance in meniscus regeneration. Therefore, SMSCs-derived EVs anticipate to provide suitable chemical cues for conferring the wet-adhesive hydrogel with the ability to promote meniscal healing via immunoregulatory potentials. Currently, there was no reports of EVs-loaded wet-adhesive being applied to meniscus repair, which is expected to achieve effective adhesion to the meniscus and exert superior promotion of meniscus repair.

In this study, we aimed to construct an antibacterial wet-adhesive hydrogel (OD/CS-PL@EVs) that was suitable to apply in the wet intra-articular microenvironment. Simultaneously, by loading SMSCs-derived EVs into the hydrogel and applying it locally through injection to the torn meniscus, we hypothesized that this composite hydrogel could promote the re-integration of the torn meniscus. The EVs were also expected to regulate local inflammation levels, recruit stem cells, and facilitate meniscal cartilage regeneration (Scheme 1).

## 2. Material and methods

### 2.1. Cell isolation and culture

Tohoku Hospital Pediatrics-1 (THP-1) was purchased from *Procell Life Science & Technology Co., Ltd.* (Shanghai, China) The cells were cultured in RPMI 1640 containing 10 % fetal bovine serum (FBS), 100 U/mL penicillin-streptomycin, and 0.05 mM 2-mercaptoethanol. The isolation of human SMSCs was approved by the Ethics Committee of the Shanghai General Hospital (2022KY068C23-1). SMSCs were harvested from the synovial tissue of patients who underwent anterior cruciate



**Scheme 1.** Fabrication of OD/CS-PL@EVs hydrogel adhesive and promotion of meniscal cartilage regeneration. A) Isolation of EVs and preparation of OD/CS-PL@EVs hydrogel adhesive. B) Injection of antibacterial OD/CS-PL@EVs hydrogel adhesive for adhesion to the meniscal lesion in the wet intra-articular micro-environment. C) The mechanism of OD/CS-PL@EVs hydrogel adhesive for meniscal cartilage regeneration. MCs and CCs represent meniscus cells and chondrocyte-like cells, respectively. C-C-SP, C-S-SP, Toll-SP, and NOD-SP represent cytokine-cytokine receptor interaction, chemokine signaling pathway, toll-like receptor signaling pathway, and NOD-like receptor pathway, respectively.

ligament reconstruction, as published methods [38]. The synovium was digested with collagenase for 4 h, and SMSCs were separated from the synovium using a 70  $\mu$ m mesh and cultured in complete medium (alpha minimum essential medium ( $\alpha$ -MEM) containing 10 % FBS and 100 U/mL penicillin-streptomycin). All experiments were conducted using SMSCs from passages 3–6. The approval for all animal experiments was obtained from the Animal Welfare & Ethics Committee of the Shanghai General Hospital (2022AW032). Rabbit meniscal cells (MCs) were isolated from healthy New Zealand white rabbits, aged 3–4 months, with a weight of 2.0–2.5 kg, based on a published manner [39]. Subsequently, identification of SMSCs was performed as described in Supplementary Information.

## 2.2. SMSCs-derived extracellular vesicles (EVs) isolation, identification and internalization

As previously described, The EVs were isolated using differential ultracentrifugation [40]. After reaching 60 % confluence, SMSCs were cultured in serum-free  $\alpha$ -MEM medium for 48 h. Subsequently, the supernatant was collected and subjected to sequential centrifugation steps: 300 g for 10 min, 2000 g for 10 min, and 10,000 g for 30 min. The supernatant was then filtered using a sterile 0.22  $\mu$ m filter. The supernatant was subjected to ultracentrifugation at  $1 \times 10^5$  g twice, each for 70 min. After discarding the supernatant, the EVs were suspended with 200  $\mu$ L PBS and stored at  $-80$  °C.

The size and concentration of EVs were calculated by Nanoparticle Tracking Analysis (NTA) (Particle Metrix, Munich, Germany). The morphology of EVs was detected using transmission electron microscope (TEM) (Thermofisher, USA). The proteins (CD9, CD63 and TSG101)

(Table S1) were measured by Western blot. According to published methods, THP-1 was induced to mature macrophage (M0), after incubation with 200 nM 12-*O*-tetradecanoylphorbol-13-acetate (PMA, Sigma, USA) for 48h [41]. SMSCs, MCs and M0 macrophages were then used for the EVs internalization studies. In brief, PKH26 (red) dye (Solarbio, China) was used to label the EVs, followed by centrifugation at  $10^5g$  to remove excess dye. The labeled EVs were incubated with cells for 48h. The cells were then fixed with 4 % paraformaldehyde (PFA), followed by staining with F-actin (Yeasen, China) and 4',6-diamidino-2-phenylindole (DAPI, Servicebio, China). A confocal microscope (Leica, Germany) was used to observe the cells.

### 2.3. Assessing EVs on the behavior of SMSCs and MCs

For cell proliferation assay, SMSCs and MCs ( $5 \times 10^3$  cells/well) were seeded in 96-well plates respectively, and treated with different concentrations of the EVs ( $0, 4 \times 10^9$  particles/mL and  $8 \times 10^9$  particles/mL). Cell Counting Kit-8 (CCK-8, Beyotime, China) was used to measure cell proliferation levels at different time points (days 1, 3 and 5). Absorbances were calculated at 450 nm by an absorbance microplate reader (BioTek Inc., USA).

For scratch test, SMSCs and MCs ( $2 \times 10^5$  cells/well) were seeded in 6-well plates respectively. When the cells reached confluence, the cell layers were scratched by 200  $\mu$ L pipette heads, followed by exposed to different concentrations of the EVs. Images were taken at 0 and 24 h using DMi8 microscope (Leica, Germany) and analyzed by ImageJ software.

For transwell test, the lower chambers were added with different concentrations of the EVs in 500  $\mu$ L serum-free medium. SMSCs and MCs ( $2 \times 10^4$  cells/well) in 200  $\mu$ L serum-free medium were seeded to the transwell upper chambers (Corning, USA) for 24 h. The upper chambers were fixed with 4 % PFA for 15 min and stained with 0.5 % crystal violet solution for 30 min. The cells were gently removed from the upper side of the chamber using cotton swabs. DMi8 microscope was used to observe the cells migrating to the downside of the chambers. The counts of migrated cells were measured by ImageJ software.

For SMSCs differentiation and MCs ECM formation, SMSCs and MCs ( $2 \times 10^4$  cells/well) were seeded in 24-well plates. After the cells reached 90 % confluence, the medium was changed to a chondrogenic medium with different concentrations of the EVs for 7 days. The cells were fixed with 4 % PFA, followed by stained with Alcian blue solution for 30 min. For immunofluorescence staining, after being fixed with 4 % PFA, the cells were exposed to 0.01 % Triton X-100. Subsequently, the cells were incubated with an anti-collagen II antibody (Table S1) at 4 °C overnight, followed by incubation with a goat anti-rabbit IgG antibody. The cells were captured under a DMi8 microscope.

For real time quantitative reverse transcription polymerase chain reaction (RT-qPCR), the total RNA from SMSCs and MCs was isolated by an RNA extraction Kit (EZBioscience, China) and subsequently reverse-transcribed to complementary DNA using a reverse transcription kit (EZBioscience, China). RT-qPCR was conducted with SYBR Green qPCR Master Mix (EZBioscience, China) following the manufacturer's instructions. mRNA expression was normalized to GAPDH, and the  $2^{-\Delta\Delta CT}$  method was employed to calculate the related gene expression. The primer sequences utilized in this study are provided in Table S2.

### 2.4. Assessing the effect and mechanism of EVs on macrophage polarization

After induced by PMA, THP-1 was then incubated with or without stimulating factors (100 ng/mL LPS and 20 ng/mL IFN- $\gamma$ ) and with different concentrations of the EVs for 72 h. For immunofluorescence, the procedures were carried out as previously described. The primary antibodies against CCR7 and Arg-1 were used to represent for M1 and M2 macrophages respectively (Table S1). Images were captured using DMi8 microscope.

For flow cytometry, the cells were stained with FITC CD86 and PE CD206 at 4 °C for 30 min in the dark. Flow cytometry was performed by LSRFortessa. The data was analyzed by Flowjo software. Antibodies were described in Table S1.

For ELISA, cytokine levels (IL-1 $\beta$ , TNF- $\alpha$ , Arg-1 and IL-10) were detected using ELISA kits according to the manufacturer's instructions.

For RT-PCR, the experiments were used to measure the expression of inflammation-related genes, including *IL-1 $\beta$* , *TNF- $\alpha$* , *Arg-1* and *IL-10* (Table S2). The instruments were as described above.

For RNA sequencing, differential gene expression of the cells was analyzed using RNA sequencing. Trizol reagent (Invitrogen) was used to extract total RNA from the cells. Gene expression showing a fold change greater than 2 and a p-value below 0.05 was considered valid. The RNA sequencing and analysis were carried out by Shanghai Biotechnology Corporation (Shanghai, China).

### 2.5. Preparation and characterization of hydrogels

Dextran (Mw = 10 kDa) and sodium periodate (NaIO<sub>4</sub>, AR, 99.5 %) were obtained from Tixiai Chemical Industry Development Co., Ltd (Shanghai, China). Carboxymethyl chitosan (83512-85-0, BR, Water solubility) was purchased from Shanghai Bangcheng Chemical Co., Ltd (Shanghai, China). Poly-L-lysine (25104-18-1) was purchased from the Shanghai Maclean Biochemical Technology Co., Ltd. 5 g of dextran was dissolved in the 80 mL distilled water, while the NaIO<sub>4</sub> (5.93 g) was dissolved in the 20 mL distilled water. Then the NaIO<sub>4</sub> solution was slowly dropped into dextran solution for 5 h of the reaction in the dark, and finally the reaction was stopped by adding 2 mL of diethylene glycol to quench the unreacted NaIO<sub>4</sub> [24]. The reaction liquid was dialyzed with a dialysis bag (relative molecular mass 3500) for 72 h, and then was freeze-dried to prepare the oxidized-dextran. The 5 mL of OD-PL (10 wt % solution in PBS, containing 2 mg/mL PL) solution, and 5 mL of CS (2 wt% solution in PBS, containing  $8 \times 10^9$ /mL EVs) were prepared to prepare the OD/CS-PL@EVs hydrogel adhesive by using a home-made double-barreled syringe with the volume ratio of 2:1. Moreover, the OD and CS solution, OD-PL and CS solution, OD and CS@EVs solution were prepared into the hydrogels and named as OD/CS, OD-PL/CS, OD/CS@EVs, respectively.

The surface morphology of OD/CS, OD-PL/CS, OD/CS@EVs, and OD/CS-PL@EVs hydrogels were analyzed by the scanning electron microscopy (SEM; Hitachi TM-1000, Japan). Briefly, the prepared adhesive hydrogels were freeze-dried, and then coated with gold for morphological assessment at an accelerating voltage of 5 kV. The mean pore size was calculated by using ImageJ (ImageJ 1.51) software based on the 500 X SEM. In addition, more characterization of hydrogels, including degradation behavior, rheology analysis, TGA, FTIR, and NMR spectroscopy analysis, gelling time testing, mechanical properties was detailed in Supplementary Information.

### 2.6. Assessing the cytocompatibility and antibacterial properties of OD/CS-PL@EVs hydrogel adhesive

Different hydrogels (OD/CS, OD/CS-PL, OD/CS@EVs, and OD/CS-PL@EVs) were prepared in sterile conditions and placed in complete medium with a concentration of 100 mg/mL to obtain the relevant extracts at 37 °C for 5 days. The cells were incubated without or with different hydrogel extracts. The absorbance was obtained using CCK-8 solution, as described above. The cytocompatibility was also analyzed by the Calcein/PI Cell Cytotoxicity Assay Kit (Beyotime, China). Photos were taken with DMi8 microscope.

Bacteria, including gram-positive *Staphylococcus aureus* (*S. aureus*) (ATCC 43300) and gram-negative *Escherichia coli* (*E. coli*) (ATCC 25922) were obtained from the American Type Culture Collection (Rockefeller, MD). Bacteria were cultured in Trypticase Soy Broth (TSB) and prepared to bacterial suspension with a concentration of  $10^7$  CFU/mL before the experiments. Different hydrogel groups (OD/CS, OD/CS-PL, OD/

CS@EVs, and OD/CS-PL@EVs) were added to a 24-well plate. 100  $\mu$ L bacterial suspension was added to the surface of different hydrogels and incubated at 37 °C for 12 h. The spread-plate method, SEM and SYTO-9/PI staining were used to study the antibacterial ability of OD/CS-PL@EVs. The detailed methods are provided in Supplementary Information.

## 2.7. Subcutaneous implantation of OD/CS-PL@EVs hydrogel adhesive

Forty SD rats were categorized into four groups, including OD/CS, OD/CS-PL, OD/CS@EVs, and OD/CS-PL@EVs, each consisting of 5 rats. The dorsal hair of the rats was shaved, and 15 mm longitudinal incisions were performed on the skin. Different hydrogel groups were subcutaneously implanted, and specimens were harvested at 2 and 4 weeks. Following fixation with PFA for 12 h, the specimens were subjected to Hematoxylin and Eosin (H&E) staining. ImageJ software was used to calculate the infiltrated cells in different groups and the remaining volume of the specimens.

## 2.8. Assessing OD/CS-PL@EVs hydrogel adhesive on the behavior of SMSCs and MCs

For the scratch test, different hydrogels (OD/CS-PL, OD/CS-PL@EVs) were added to the upper chamber with 200  $\mu$ L. For transwell test, the lower chamber was supplemented with 200  $\mu$ L of different hydrogels in a 500  $\mu$ L medium. The cells were incubated with hydrogels for 24 h and observed using a DMi8 microscope at 0 h and 24 h.

According to the above descriptions, the cells were incubated with different hydrogels for 7 days. The cells were then stained with Alcian blue solution or anti-collagen II antibody, as described above. The cells were taken under a DMi8 microscope. The expression of chondrogenic-related genes was analyzed using RT-qPCR.

## 2.9. Assessing OD/CS-PL@EVs hydrogel adhesive on macrophage polarization

M0 macrophage was seeded to the down chamber of 24-well plates with or without stimulating factors. The upper chamber was added with or without 200  $\mu$ L hydrogels. The cells were incubated with the primary antibodies to CCR7 and Arg-1 for immunofluorescence. For flow cytometry, the cells were incubated with CD86 and CD206 antibodies and analyzed using LSRFortessa. For ELISA, the cytokine levels were detected using ELISA kits, including IL-1 $\beta$ , TNF- $\alpha$ , Arg-1 and IL-10. Inflammation-related gene expression was calculated by RT-PCR.

## 2.10. Meniscal defect model in rabbit

A total of 40 mature male rabbits (New Zealand White rabbits, 3.0 kg) were used in this study. The bilateral knee joints of each rabbit were involved in the animal experiments. All rabbits were randomly allocated into four groups as follows: the control group, OD/CS-PL group, OD/CS-PL@EVs group, and sham group. The surgery was conducted under inhalation anesthesia using isoflurane. The knee area was shaved and cleaned using chlorhexidine gluconate. A medial parapatellar incision was made and the cylindrical defect (1.5-mm diameter) was created in the inner two-thirds of the anterior portion of the medial meniscus by a skin biopsy punch (Kai Medical). Subsequently, 200  $\mu$ L of OD/CS-PL@EVs was implanted in the right knee (OD/CS-PL@EVs group) with the dual syringe. The left knee was implanted with or without 200  $\mu$ L of OD/CS-PL (OD/CS-PL group and the control group). The sham group procedure, which included exposing the medial joint and subsequent closure in layers without creating defect, was conducted in the right knee.

## 2.11. Histologic evaluation and biomechanical testing

The menisci, femoral condyle (FC) and tibial plateau (TP) were harvested at 1 week, 6 weeks and 12 weeks after surgery in each knee respectively, followed by photography and observation. FC and TP were evaluated using The International Cartilage Repair Society (ICRS) cartilage lesions classification [42].

For histological evaluation, the menisci, harvested 1 week after surgery was fixed with 10 % neutral buffered formalin (Servicebio, China), followed by dehydrated and embedded in paraffin to cut to sections. The sections were then prepared for immunofluorescence staining with TNF- $\alpha$  and IL-10 (Table S1). The immunofluorescence intensity was measured by ImageJ software.

The menisci, FC, and TP harvested at 6 weeks and 12 weeks after surgery were also prepared into sections. The sections of menisci were then stained with H&E, safranin O (S-O), toluidine blue (TB) and Col II. FC and TP were sectioned by the methods as previously described [43]. The sections were stained with H&E and TB and then graded blindly using the Mankin grading system [44]. ImageJ software was used to analyze the deposition of Col II semi-quantitatively.

For biosafety evaluation *in vivo*, the organs (heart, spleen, liver, kidney, lung) in rabbits of each group were collected, fixed with PFA, and subsequently embedded in paraffin and stained with H&E.

The medial menisci from each group were harvested and placed at 4 °C. (the control group, OD/CS-PL group, OD/CS-PL@EVs group, and the sham group) (n = 5) at week 12. For biomechanical testing, the healed tissue and surrounding normal tissue were cut into a rectangular specimen (3 mm  $\times$  3 mm; thickness,  $\sim$ 2.2–2.5 mm). The compression testing of regenerated menisci was performed to measure the compressive stress by the universal testing machine equipped with a 100 N load cell at a crosshead speed of 1 mm/min.

## 2.12. Statistical analysis

The data are expressed as mean  $\pm$  standard deviation (SD). GraphPad Prism 8.0 (GraphPad Software Inc., USA) was utilized for statistical analysis. In each experiment, statistical analysis was conducted using a minimum of three independent samples. Statistical significance was analyzed using One-way analysis of variance (ANOVA) or Student's t-test. The Tukey method was employed for post-hoc analysis. Statistical significance was defined at a threshold of P < 0.05.

## 3. Results

### 3.1. Characterization of SMSCs and EVs

To begin with, the isolated cells showed a typical spindle-shaped morphology under the microscope (Fig. 1A). After culturing in osteogenic, adipogenic, and chondrogenic media for 3 weeks, the cells respectively formed calcium deposition, lipid droplets, and proteoglycans, demonstrating their capability for trilineage differentiation (Fig. 1B). As shown in Fig. 1C–E, flow cytometry of surface antigens on these cells showed that over 90 % were positive for CD44 and CD90, while CD34 was mainly negative. These above results suggested that SMSCs were isolated.

Furthermore, after removing cells and cell debris from the supernatant (Fig. 1G), transmission electron microscopy (TEM) demonstrated that the obtained products exhibited a classic cup-shaped or semi-spherical morphology with bilayer membranes (Fig. 1I). The results of nanoparticle tracking analysis (NTA) indicated that the average diameter of EVs was (140  $\pm$  41) nm (Fig. 1F). Moreover, Western blot analysis showed high expression levels of the surface markers TSG101, CD9, and CD63 on the products (Fig. 1H). Hence, the prepared products should belong to SMSC-derived EVs. Next, we evaluated the 48h internalization of EVs in SMSCs, MCs and M0 macrophage induced from THP-1. These EVs could be internalized and were found to be abundant

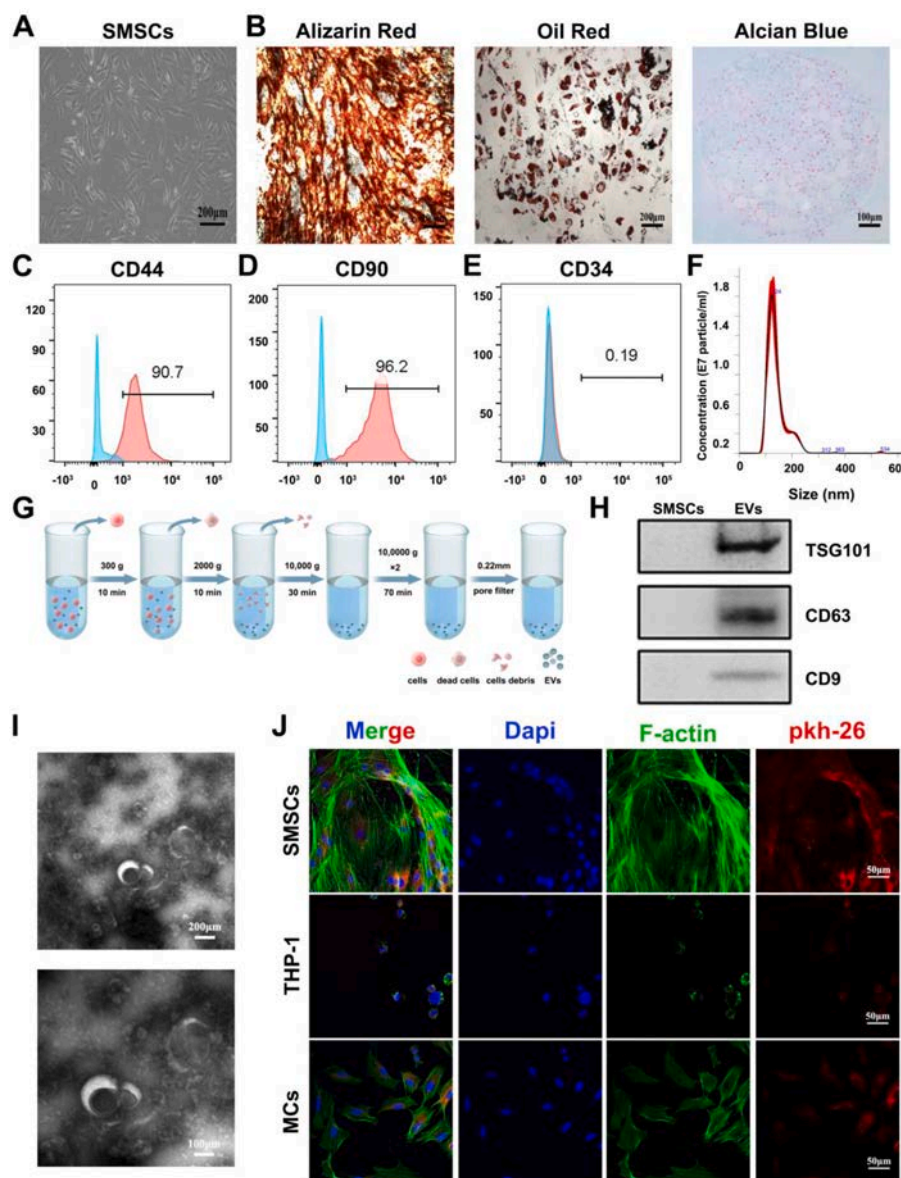


**Fig. 1.** Identification and internalization of SMSCs and EVs. A) Picture of SMSCs. Scale bar = 200  $\mu\text{m}$ . B) Representative images of Alizarin red, Oil Red O, and Alcian blue staining. Scale bar = 200 or 100  $\mu\text{m}$ . C-E) Flow cytometry pictures of SMSCs surface markers CD90, and CD44, with CD34 as negative control. F) Particle size distribution of EVs measured by NTA. G) Schematic illustration of EVs isolation. H) Western blot of EVs-related markers including CD63, TSG101, and CD9. I) EVs morphology taken by TEM. Scale bar = 200 or 100  $\mu\text{m}$ . J) PKH-26-labeled EVs internalized by THP-1, SMSCs and MCs. Scale bar = 50  $\mu\text{m}$ .

within these cells (Fig. 1J). The results demonstrated that SMSC-derived EVs were successfully prepared and could interact with intra-articular cells.

### 3.2. Response of SMSCs and MCs to EVs

Cell viability assays were performed after SMSCs and MCs co-cultured with EVs for 1, 3, and 5 d respectively. As shown in Fig. 2A–B, the results indicated that EVs significantly enhanced the absorbance of both SMSCs and MCs time-dependently, with the enhancement effect positively correlated with the concentration of EVs at each time point.

Scratch assay and Transwell assay were further carried out to assess the effect of EVs on SMSCs and MCs migration. The cells from different groups were cultured for 24 h, and the scratch width was recorded at 0 h and 24 h after scratching, along with the number of cell migration at 24 h. As shown in Fig. 2C–F, the EVs group exhibited a significantly smaller scratch width, indicating faster cell migration, which was associated

positively with the concentration of EVs. Additionally, the results of the Transwell assay (Fig. 2G–J) demonstrated that the migrated cells in the EVs group were significantly more than those in the control group. These findings indicated that EVs significantly enhance the migration capability of SMSCs and MCs.

We used Alcian staining, immunofluorescence, and RT-qPCR to investigate the effect of EVs on the chondrogenic differentiation of SMSCs and MCs ECM formation. As shown in Fig. 2K–L, the proteoglycan expression in the EVs groups with different concentrations was increased after incubation with EVs for 7 d in a concentration-dependent manner. Additionally, the immunofluorescence staining results for Col II showed significantly enhanced intensity of red fluorescence in EVs-treated SMSCs and MCs, indicating that EVs significantly promoted the secretion of Col II in both SMSCs and MCs, as shown in Fig. 2M–N. Similarly, as shown in Fig. 2P–Q, semi-quantitative analysis of immunofluorescence staining also supported the results.

Furthermore, mRNA was extracted from SMSCs and MCs in each group, and RT-qPCR was used to evaluate the mRNA expression levels of

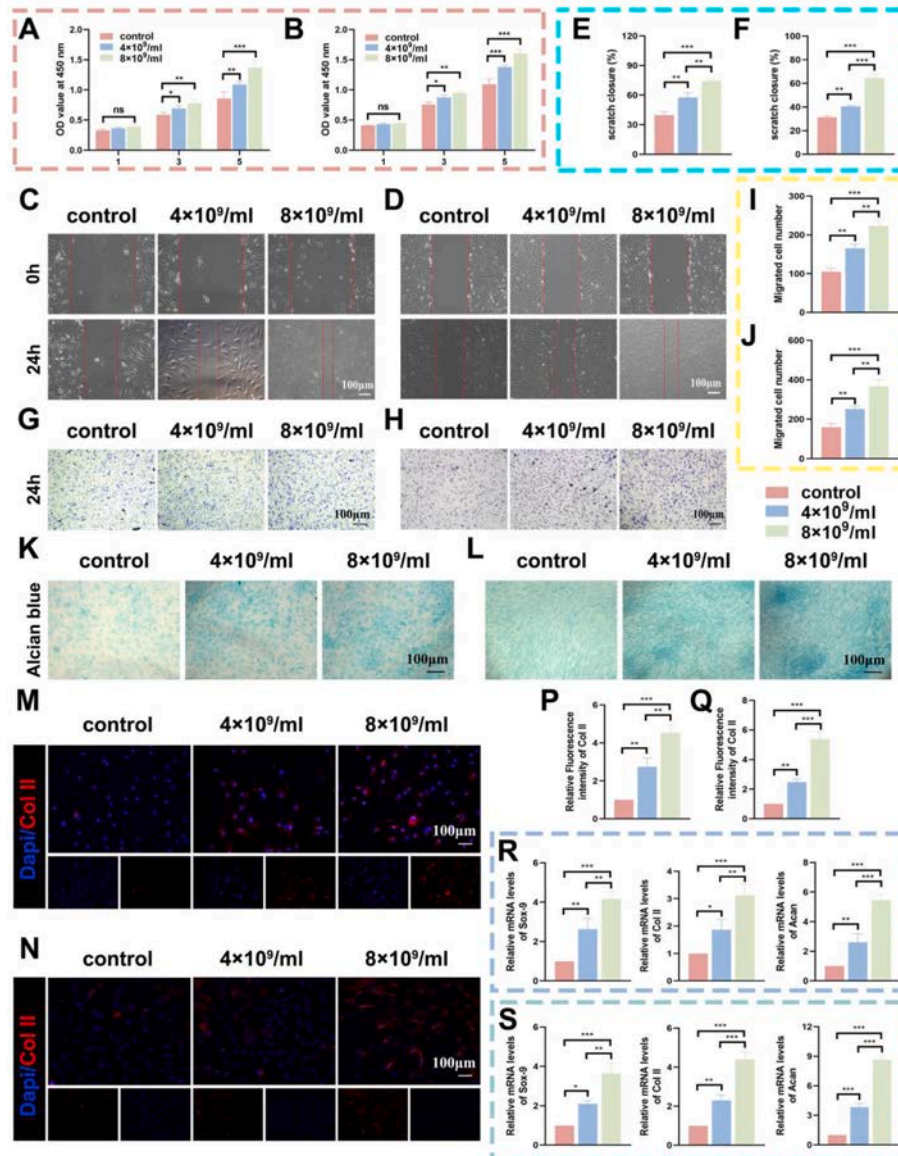


**Fig. 2.** The influence of EVs for SMSCs differentiation and ECM formation of MCs. A-B) Effect of EVs on the proliferation of SMSCs and MCs measured by CCK-8 assay, respectively. C-D) Representative images of SMSCs and MCs migration evaluated by scratch assay, respectively. E-F) Semi-quantitative analysis of SMSCs and MCs scratch assay, respectively. G-H) Representative images of SMSCs and MCs Transwell assay treated with different concentrations of EVs, respectively. I-J) Semi-quantitative analysis of SMSCs and MCs Transwell assay, respectively. K-L) Representative images of SMSCs and MCs Alcian Blue staining, respectively. M – N) Representative immunofluorescence images of Col II expressed by SMSCs and MCs, respectively. P-Q) Relative fluorescence intensity of Col II expressed by SMSCs and MCs, respectively. R–S) The mRNA expression of chondrogenic genes in SMSCs and MCs measured by RT-qPCR. Scale bar = 100  $\mu$ m ns represents no significance. \* $p < 0.05$ , \*\* $p < 0.01$ , \*\*\* $p < 0.001$ .

chondrogenic-related genes, including *Col II*, *aggrecan (Acan)*, and *Sox-9*. The results showed that after 7 d co-culture, EVs significantly increased the mRNA expression levels of *Col II*, *Acan*, and *Sox-9* in SMSCs and MCs in a concentration-dependent manner (Fig. 2R–S). These results collectively demonstrated that EVs intervention promoted chondrogenic differentiation of SMSCs and enhanced the formation of cartilaginous ECM in MCs.

### 3.3. The effects of EVs on the polarization of macrophage and associated molecular mechanisms

To investigate the regulatory effects of EVs on the polarization of macrophages, M0 macrophage was induced from THP-1 using PMA, and then intervened with stimulating factors (SF, 100 ng/mL LPS and 20 ng/mL IFN- $\gamma$ ) into M1 phenotype. Firstly, to demonstrate the alterations in

macrophage phenotypes, we used immunofluorescence staining for CCR7 and Arg-1, representing M1 and M2 phenotypes, respectively. As indicated in Fig. 3A and C, the group intervened with only SF exhibited extensive overexpression of CCR7 and low expression of Arg-1 compared to the control group. Notably, the CCR7 expression was significantly reduced, while Arg-1 was significantly increased by EVs treatments in a concentration-dependent manner. Moreover, consistent results were obtained through semi-quantitative analysis of fluorescence intensity (Fig. 3B and D). In addition, we employed flow cytometry to analyze the polarization of macrophage. As depicted in Fig. 3E and F, the group treated solely with SF exhibited the highest ratio of M1 phenotype and a low ratio of M2 phenotype. However, the proportion of the M1 phenotype significantly decreased, while the proportion of the M2 phenotype increased markedly with the addition of EVs, and this shift was more evident with increasing concentrations of EVs. The analysis of the mean

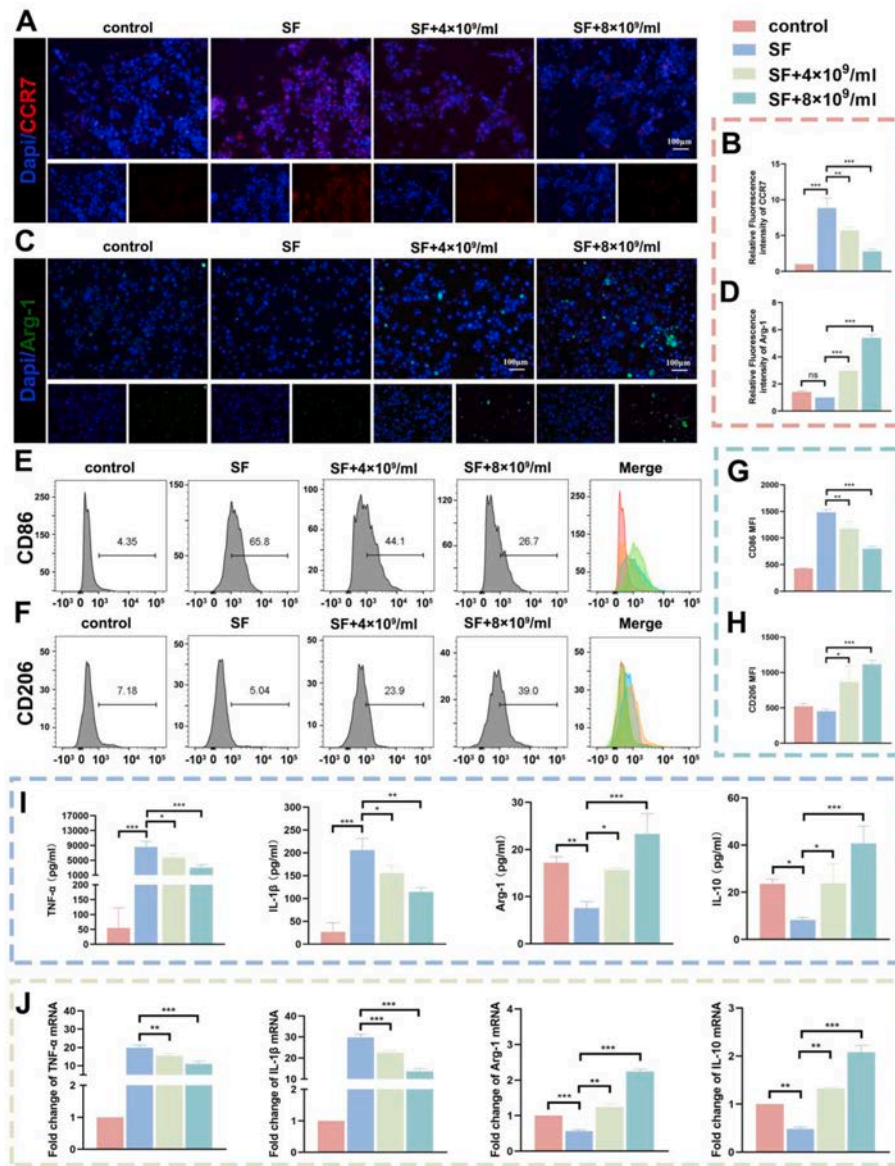


**Fig. 3.** EVs modulated the polarization of macrophages from M1 to M2 phenotype. A-B) Representative immunofluorescence images and relative fluorescence intensity of CCR7 (red) expressed by macrophages. C-D) Representative immunofluorescence images and relative fluorescence intensity of Arg-1 (green) expressed by macrophages. E-F) Representative flow cytometry of macrophage markers CD86 (M1) and CD206 (M2). G-H) Mean fluorescence intensity of CD86 and CD206 measured by flow cytometry. I) The inflammatory cytokines expression of macrophage measured by ELISA. J) The mRNA expression of inflammatory genes measured by RT-qPCR. Scale bar = 100  $\mu$ m ns represents no significance. \* $p < 0.05$ , \*\* $p < 0.01$ , \*\*\* $p < 0.001$ . "SF" represents stimulating factors (100 ng/mL LPS and 20 ng/mL IFN- $\gamma$ ).

fluorescence intensity (MFI) for each group also revealed a consistent trend in the results (Fig. 3G-H). Thus, EVs had the capability of facilitating macrophage polarization from M1 to M2 phenotype.

We then conducted ELISA and RT-qPCR experiments to evaluate the expression levels of pro-inflammatory (TNF- $\alpha$ , IL-1 $\beta$ ) and anti-inflammatory (Arg-1, IL-10) cytokines and genes in different experimental groups. As shown in Fig. 3I-J, the pro-inflammatory cytokines and genes were significantly upregulated in the SF group, while the anti-inflammatory cytokines and genes were significantly downregulated compared to the control group. In contrast, the EVs treatment group exhibited a significant downregulation of TNF- $\alpha$  and IL-1 $\beta$  cytokines secretion and gene expression, along with a significant upregulation of Arg-1 and IL-10 cytokines secretion and gene expression compared to the SF group. In addition, the higher concentration of EVs exhibited better regulation capabilities.

To further explore the molecular mechanisms of macrophage

polarization regulated by EVs, we performed RNA sequencing on macrophages subjected to two treatments, including SF treatment and SF + EVs treatment. SF group was designated as the control group. There were significant differences in RNA expression between SF group and SF + EVs group, as indicated by the results of principal component analysis (PCA) (Fig. 4A). Heatmaps and volcano plots were further generated, exhibiting 586 upregulated genes and 610 downregulated genes in SF + EVs group compared to SF group (Fig. 4B-C). GO enrichment analysis was conducted and the results indicated that the differentially expressed genes were mainly associated with immune system processes and inflammatory responses (Fig. 4D). KEGG enrichment analysis further showed significant differences in gene expression, such as cytokine-cytokine receptor interaction, chemokine signaling pathway, toll-like receptor signaling pathway, and NOD-like receptor pathway after EVs treatment compared to the control group (Fig. 4E). Genes in these pathways were significantly downregulated in the SF + EVs group, and

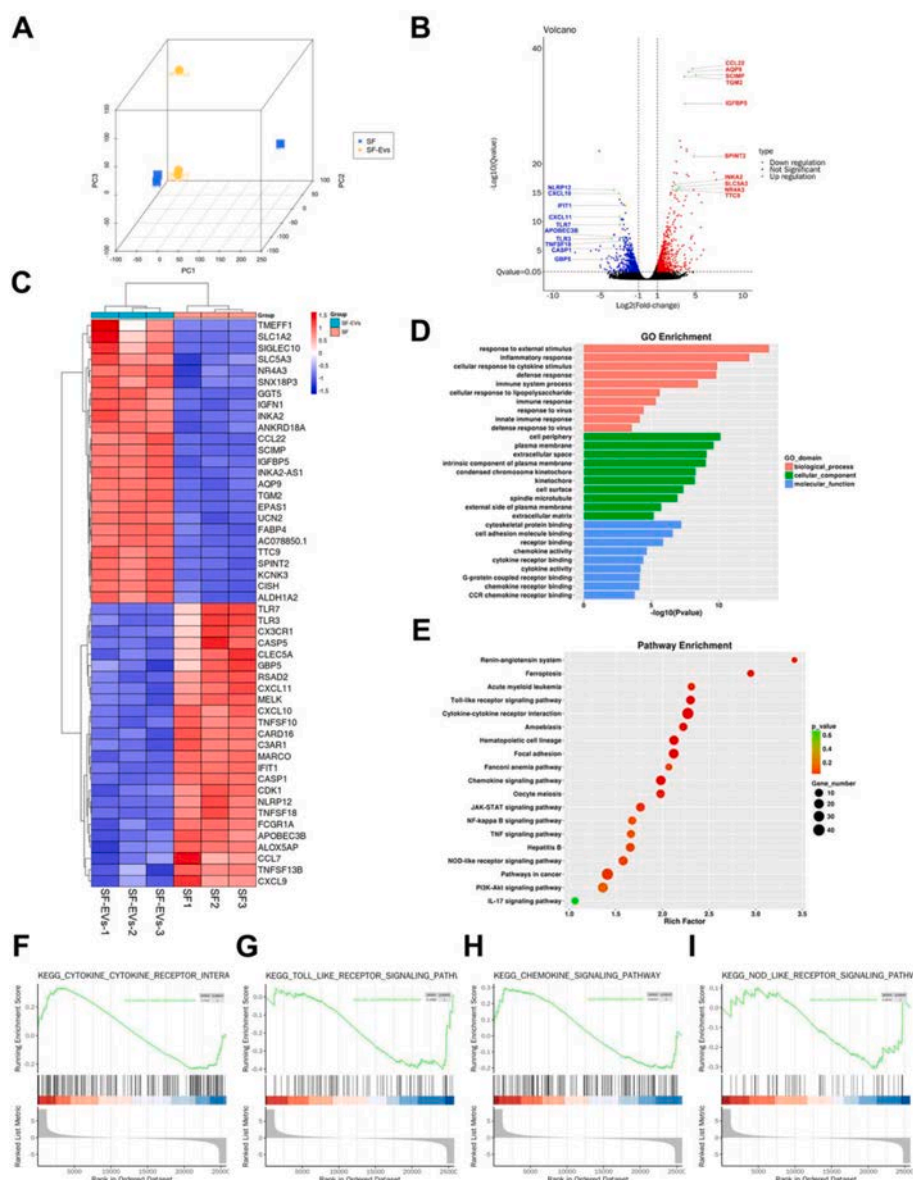


**Fig. 4.** Molecular mechanisms of EVs modulation the macrophage polarization. A) Principal component analysis (PCA) of each group. B–C) Volcano map and Heat map of differential genes between SF + EVs and SF group related to enrichment pathway. D) Top 30 of differential genes by GO enrichment analysis between SF + EVs and SF group. E) Top 20 the differential pathway by KEGG enrichment analysis between SF + EVs and SF group. F–I) GSEA enrichment analysis of cytokine-cytokine receptor interaction, chemokine signaling pathway, toll-like receptor signaling pathway, and NOD-like receptor pathway between SF + EVs and SF group.

were further confirmed in volcano plots and heatmap. Moreover, GSEA results confirmed the downregulation of cytokine-cytokine receptor interaction, chemokine signaling pathway and toll-like receptor signaling pathway, and NOD-like receptor pathway after EVs intervention (Fig. 4F–I), which was consistent with the KEGG results. Therefore, EVs showed the immunoregulatory efficacy of inflammation via macrophage polarization from M1 to M2 phenotype.

### 3.4. Preparation and characterization of OD/CS-PL@EVs hydrogel adhesive

To prepare the OD/CS-PL@EVs hydrogel adhesive, the oxidized dextran (OD) was synthesized and characterized by FTIR, TGA, and NMR. The FTIR spectrum showed the broad band of  $3800\text{--}3000\text{ cm}^{-1}$  in the infrared absorption spectra of OD, which was narrower than the dextran due to the hydroxyl group content decreasing, while the new absorption peak appeared at  $1733\text{ cm}^{-1}$  due to the forming hemiacetal structure (Fig. 5A). Meanwhile, the TGA displayed the OD possessed a

lower degradation temperature of around  $200\text{ }^{\circ}\text{C}$  than that of dextran around  $270\text{ }^{\circ}\text{C}$  (Fig. 5B), while the NMR spectrum showed the characteristic proton signals from aldehyde groups ( $9.2\text{--}9.1\text{ ppm}$ ) and hemiacetal groups ( $6.0\text{--}4.1\text{ ppm}$ ), as demonstrated in Fig. 5C. Moreover, the oxidation degree of oxidized dextran was  $78.21 \pm 4.14\%$ . Altogether, these results indicated the dextran was successfully oxidized to obtain the OD.

Afterwards, all hydrogels were prepared with the double-linked syringes. To prepare the OD/CS-PL@EVs hydrogels, the 10 % OD concentration could form a gel quickly to full the meniscus defect with suitable anti-stress properties, while the 2 % CS displayed suitable solubility characteristics and fluidity. As shown in Fig. 5D, the prepared OD/CS and OD/CS@EVs hydrogels were colorless transparent appearance, while the OD/CS-PL and OD/CS-PL@EVs hydrogels showed slight milky white cloudiness due to inducing PL leading to the increasing degree of cross-linking. Meanwhile, the scanning electron microscopy (SEM) also indicated all hydrogels displayed a porous structure, the mean pore sizes were  $58.9 \pm 14.5\text{ }\mu\text{m}$ ,  $59.0 \pm 12.2\text{ }\mu\text{m}$ ,  $47.8 \pm 13.6\text{ }\mu\text{m}$

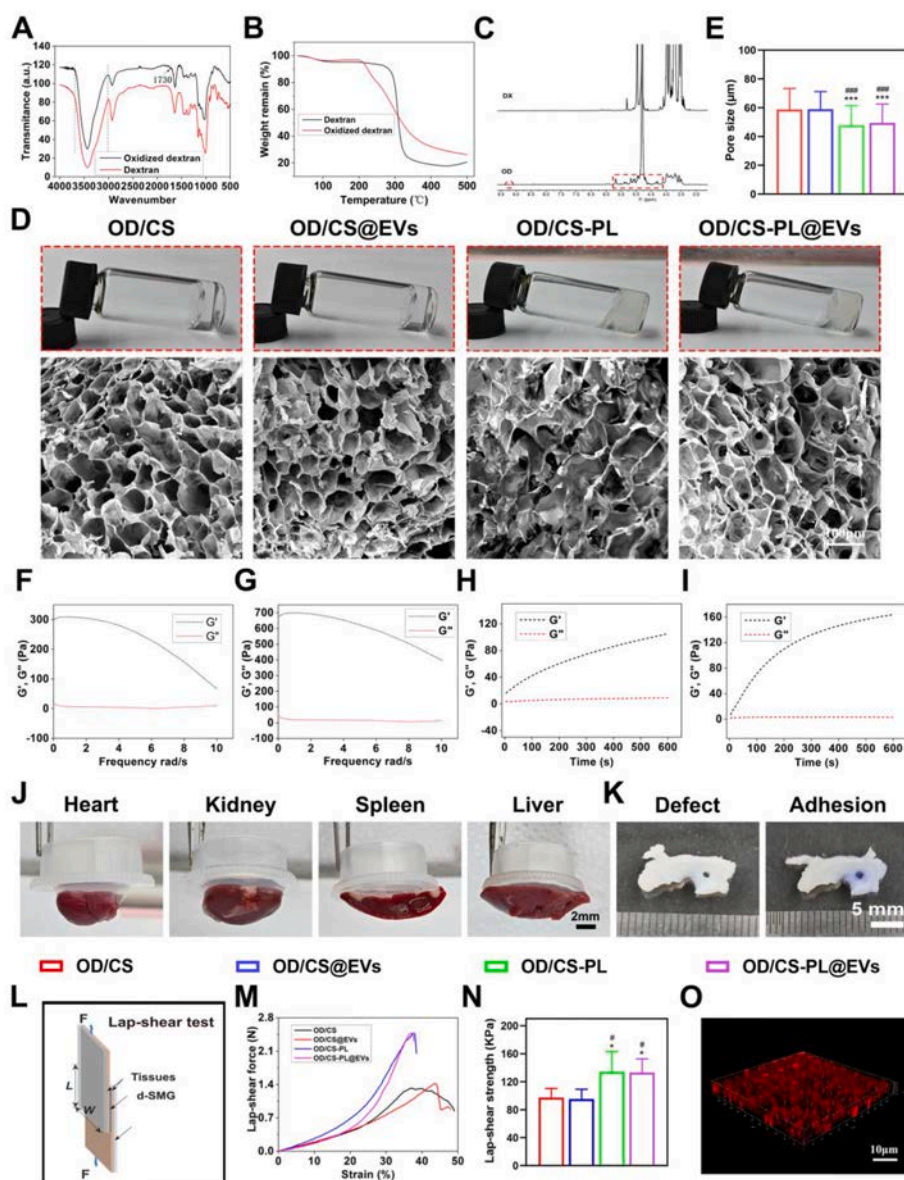


**Fig. 5.** Characterization of physicochemical properties of hydrogels. A) Fourier transform infrared (FTIR) spectra of dextran and oxidized dextran. B) Weight remains of dextran and oxidized dextran assessed by Thermo-gravimetric Analyzer (TGA). C) NMR spectra of dextran and oxidized dextran. D) Macroscopic appearance and SEM of different hydrogels. Scale bar = 100  $\mu\text{m}$ . E) Pore size of different hydrogels. F, H) The rheological property assay of OD/CS. G, I) The rheological property assay of OD/CS-PL hydrogel adhesive to different tissues. J) The adhesion property of OD/CS-PL@EVs hydrogel adhesive to meniscal tissues before and after injecting to the meniscal defect site. K) The adhesion property of OD/CS-PL@EVs hydrogel adhesive measured by lap-shear testing. L) The adhesion mechanics of hydrogels by the lap-shear testing. M) The lap shear stress–strain curves of different hydrogels. N) The adhesion strength of different hydrogels. O) EVs distribution in OD/CS-PL@EVs hydrogel adhesive measured by confocal microscopy. Scale bar = 10  $\mu\text{m}$ . \* $p < 0.05$  and \*\*\* $p < 0.001$ , when compared to OD/CS group. # $p < 0.05$  and ### $p < 0.001$ , when compared to OD/CS@EVs group.

and  $49.6 \pm 13.0 \mu\text{m}$  for OD/CS, OD/CS@EVs, OD/CS-PL and OD/CS-PL@EVs hydrogels, which showed these hydrogels possessed large pore size for facilitating cell infiltration (Fig. 5E). Moreover, the OD/CS-PL and OD/CS-PL@EVs hydrogels showed smaller pore sizes than the OD/CS, OD/CS@EVs hydrogels. Meanwhile, the gelatinization time were respectively  $32.6 \pm 3.6\text{s}$ ,  $33.2 \pm 5.4\text{s}$ ,  $22.8 \pm 4.9\text{s}$ , and  $21.8 \pm 4.8\text{s}$  for OD/CS, OD/CS@EVs, OD/CS-PL and OD/CS-PL@EVs hydrogels (Fig. S1). All these examinations revealed the PL increased the cross-linking degree.

The *in vitro* degradation features of these hydrogels showed all samples displayed increasing in mass due to the swollen stream water of the hydrogel itself in the first three days, and then the hydrogels appeared a drop tendency. The maximum swelling ratio was respectively  $115.7 \pm 5.5\%$ ,  $116.1 \pm 6.7\%$ ,  $114.9 \pm 7.5\%$ , and  $113.9 \pm 4.1\%$

at 36 h, while the remained mass was respectively  $39.9 \pm 7.4\%$ ,  $39.2 \pm 5.9\%$ ,  $46.0 \pm 10.9\%$ ,  $45.8 \pm 12.1\%$  for OD/CS, OD/CS@EVs, OD/CS-PL and OD/CS-PL@EVs hydrogels at 35 d, which showed these hydrogels displayed the low swelling rate and a relatively long degradation cycle (Fig. S2). As a trace addition, EVs didn't change the physical and chemical properties, thus, the viscosity and mechanical properties of OD/CS, and OD/CS-PL hydrogels were employed by the rheological property assay, which the results presented the OD/CS-PL hydrogel displayed lower rigidity and better elastic deformability than that in the OD/CS hydrogel, as shown in Fig. 5F–I and Fig. S3.

We further assessed the compressive properties of hydrogels, the strain-stress curve showed all hydrogels presented similar compressive stress mode, while the mechanical behavior of OD/CS-PL and OD/CS-PL@EVs hydrogels was better than that of OD/CS and OD/CS@EVs

hydrogels. Then, the quantitative analysis displayed the broken strain was  $26.66 \pm 5.55\%$ ,  $26.66 \pm 5.52\%$ ,  $29.42 \pm 3.80\%$ , and  $28.21 \pm 5.78\%$ , as well as the maximum compressive strength was  $6.88 \pm 1.39$  KPa,  $7.26 \pm 1.26$  KPa,  $10.55 \pm 2.08$  KPa, and  $10.05 \pm 1.08$  KPa for OD/CS, OD/CS@EVs, OD/CS-PL and OD/CS-PL@EVs hydrogels (Fig. S4), which showed the PL could significantly improve the compressive mechanical properties of hydrogels.

Moreover, as shown in Fig. 5J, the OD/CS-PL@EVs hydrogels could adhere well to different tissues, and bear their own weight without falling off, showing excellent *ex vivo* adhesion characteristics. Meanwhile, as demonstrated in Fig. 5K, the cylindrical defect was prepared throughout the meniscus, and the *in-situ* filling of the defect could be achieved by injection of OD/CS-PL@EVs hydrogels. Quantitative analysis of the adhesion mechanics of hydrogels by the lap-shear testing (Fig. 5L), the lap shear stress–strain curves showed the hydrogels

without PL (OD/CS, OD/CS@EVs), and with PL (OD/CS-PL, OD/CS-PL@EVs) hydrogels had different dopamine grafting ratios (Fig. 5M). The adhesion strength was  $97.67 \pm 12.76$  KPa,  $95.52 \pm 13.86$  KPa,  $134.45 \pm 28.69$  KPa, and  $133.08 \pm 19.62$  KPa for OD/CS, OD/CS@EVs, OD/CS-PL and OD/CS-PL@EVs hydrogels, which showed PL increased the adhesion mechanics of the hydrogel (Fig. 5N). Besides, EVs with red fluorescence (PKH-26) were observed under a confocal microscope, indicating the even distribution of EVs within the OD/CS-PL@EVs hydrogel (Fig. 5O). These above results together indicated the advantageous *in vitro* and *ex vivo* mechanical performances of the prepared OD/CS-PL@EVs hydrogels.

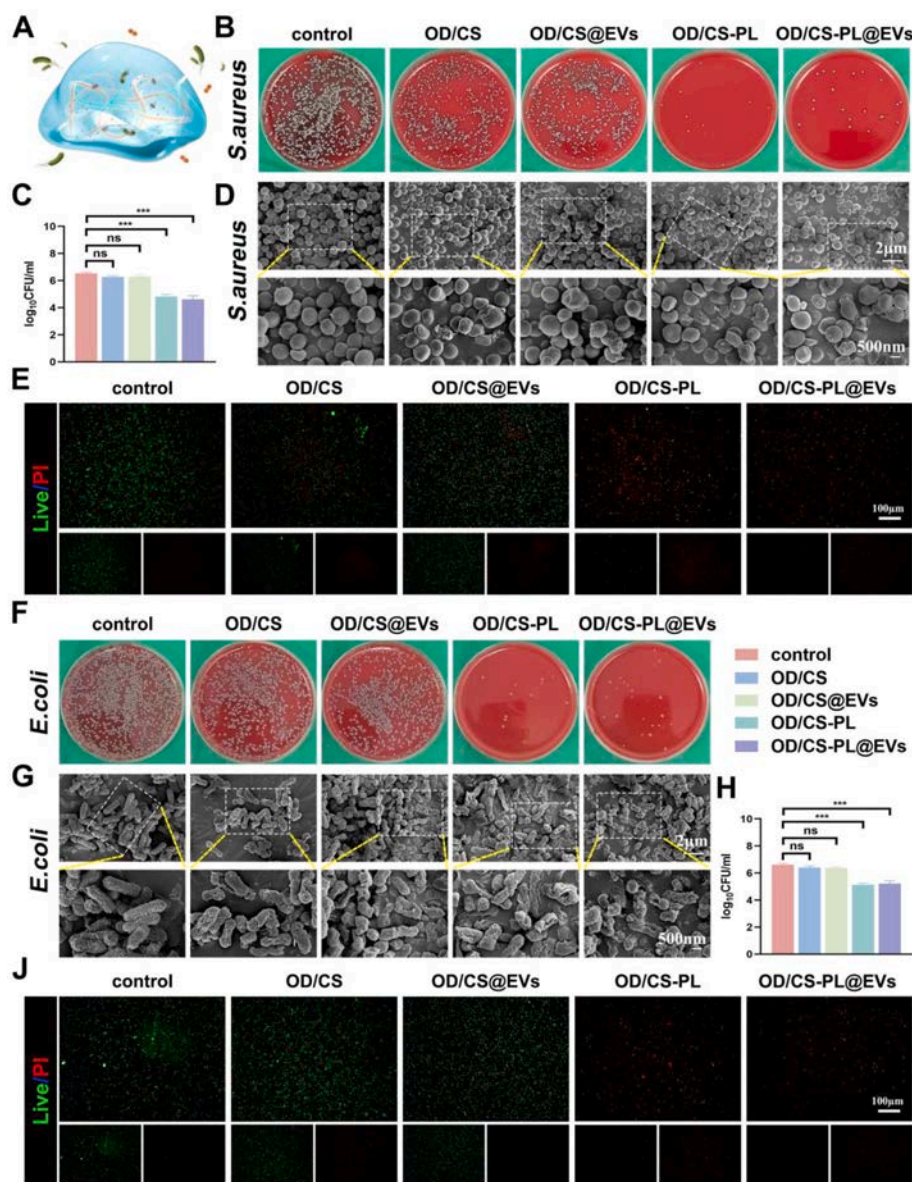


**Fig. 6.** Antibacterial effect of OD/CS-PL@EVs hydrogel adhesive against *S. aureus* and *E. coli*. A) Schematic illustration of different hydrogels against *S. aureus* and *E. coli*; (B–C) Representative images of *S. aureus* colonies and antibacterial efficiency under different treatments (saline, OD/CS, OD/CS@EVs, OD/CS-PL, and OD/CS-PL@EVs). D) Representative SEM images of *S. aureus* under different treatments. E) Representative Live/Dead Fluorescent images of *S. aureus* treated in different ways. (green signal: living bacteria; red: dead bacteria). F, H) Representative images of *E. coli* colonies and antibacterial efficiency under different treatments. G) Representative SEM images of *E. coli* under different treatments. J) Representative LIVE/DEAD Fluorescent images of *E. coli* treated in different ways. Scale bar = 100  $\mu$ m, 2  $\mu$ m or 500 nm ns represents no significance. \* $p < 0.05$ , \*\* $p < 0.01$ , \*\*\* $p < 0.001$ .

### 3.5. The cytocompatibility and antibacterial properties of OD/CS-PL@EVs hydrogel adhesive

We evaluated the cytocompatibility of the prepared hydrogels with different components (OD/CS, OD/CS-PL, OD/CS@EVs, and OD/CS-PL@EVs). SMSCs and MCs were co-cultured with the extracts of OD/CS, OD/CS-PL, OD/CS@EVs, and OD/CS-PL@EVs for 5 d. Live/dead fluorescence staining was performed on SMSCs and MCs, as shown in Figs. S5A–B. The results indicated that SMSCs and MCs exhibited normal growth, with spindle-shaped cell morphology in all groups. Meanwhile, SMSCs and MCs in OD/CS@EVs and OD/CS-PL@EVs groups were found more than those in OD/CS and OD/CS-PL groups. The absorbance of SMSCs and MCs was then measured using CCK-8 assay kit to evaluate cell viability, and the OD/CS@EVs and OD/CS-PL@EVs group significantly promoted the proliferation of both SMSCs and MCs, while the OD/CS and OD/CS-PL groups did not exhibit a noticeable proliferative effect on SMSCs and MCs (Figs. S5C–D). It was concluded that the proliferation of the cells was promoted by the loaded EVs in OD/CS-PL@EVs hydrogels.

Gram-positive bacteria *S. aureus* and gram-negative *E. coli* were selected to assess the antibacterial performance of different hydrogels (Fig. 6A). Fig. 6B–C and F, H indicated that after co-culturing with bacteria for 12 h, the OD/CS and OD/CS@EVs groups did not show significant antibacterial effects, while the OD/CS-PL and OD/CS-PL@EVs groups exhibited superior antibacterial ability against *S. aureus* and *E. coli*. It is worth noting that the introduction of PL into OD/CS significantly enhanced the antibacterial effects of the hydrogel, achieving superior antibacterial efficacy against both *S. aureus* and *E. coli*. Next, morphological changes of *S. aureus* and *E. coli* after co-culturing with hydrogels were observed using SEM. As shown in Fig. 6D and G, *S. aureus* and *E. coli* exhibited spherical and rod-shaped forms with smooth surfaces and intact cell walls in the control group, while the bacterial morphology in the OD/CS and OD/CS@EVs groups showed distortion, and cell walls appeared wrinkled to some extent. Furthermore, in the OD/CS-PL and OD/CS-PL@EVs groups, both bacterial morphology and cell walls were further distorted and damaged. The live/dead fluorescence staining experiment further identified the antibacterial effects of hydrogels. The OD/CS-PL and OD/CS-PL@EVs groups had a higher number of dead *S. aureus* and *E. coli* compared to the other groups (Fig. 6E and J). All these results indicated that OD/CS-PL@EVs exhibited obvious antibacterial capabilities against both *S. aureus* and *E. coli*, providing strong support for next-step tissue regeneration.

### 3.6. Degradation and cell infiltration of OD/CS-PL@EVs hydrogel adhesive in subcutaneous implantation model

To investigate the cell infiltration effect after implantation *in vivo*, we implanted different hydrogels (OD/CS, OD/CS-PL, OD/CS@EVs, and OD/CS-PL@EVs) subcutaneously in rats. Firstly, all hydrogel groups exhibited a mild immune response (Figs. S6A–B). At week 2, the OD/CS and OD/CS-PL groups showed several layers of infiltrated cells at the edges, while a dense hydrogel structure was visible in the central region, suggesting that OD/CS and OD/CS-PL facilitated cell infiltration. In contrast, the OD/CS@EVs and OD/CS-PL@EVs groups exhibited some gaps in the central region, and more cells infiltrated. This indicated that the introduction of EVs into the hydrogel promoted cell infiltration and hydrogel degradation. At week 4, the OD/CS and OD/CS-PL groups exhibited increased cell infiltration and decreased hydrogel volume compared to the 2-week time point. In contrast, the OD/CS@EVs and OD/CS-PL@EVs groups demonstrated a higher level of cell infiltration and a smaller residual volume than the other groups. These findings indicated that EVs could promote cell recruitment within the hydrogel and the hydrogel degradation. We further conducted a semi-quantitative analysis of cell infiltration quantity and remaining hydrogel volume (Figs. S6C–D). The results also showed that the presence of EVs

significantly promoted the cell infiltration ability of the hydrogel, as well as the degradation rate of the hydrogel.

### 3.7. Response of SMSCs and MCs to OD/CS-PL@EVs hydrogel adhesive

To further investigate the impact of hydrogels on the migration ability of SMSCs and MCs, we co-cultured OD/CS-PL and OD/CS-PL@EVs with SMSCs and MCs, and evaluated the migration potential by scratch assays and migration experiments. Fig. 7A and C demonstrated that the OD/CS-PL@EVs group significantly promoted the reduction of scratch width in SMSCs, while the OD/CS-PL group did not show a significant decrease in scratch width compared to the control group. The ability of OD/CS-PL@EVs to promote cell migration was also confirmed in MCs results (Fig. 7B and D). Additionally, in the Transwell experiments, OD/CS-PL@EVs group significantly promoted the migration of SMSCs to the down surface of the chamber compared to the control group and the OD/CS-PL group, while the migration of SMSCs in the OD/CS-PL group showed no significant difference from the control group (Fig. 7E and G). Similar results are also observed in MCs as well (Fig. 7F and H). These results proved that the prepared OD/CS-PL@EVs has a superior ability to promote SMSCs and MCs migration.

As shown in Fig. 7I–J, the proteoglycan expression analyzed by Alcian staining of SMSCs and MCs in the OD/CS-PL@EVs group were significantly more than those in the control and OD/CS-PL groups at 7 d, while the OD/CS-PL group had similar proteoglycan expression to the control group. The immunofluorescence intensity of Col II in the OD/CS-PL@EVs group was higher than that in the control and OD/CS-PL groups. The control group and OD/CS-PL group had similar fluorescence intensity (Fig. 7K–L). The results were further confirmed by fluorescence semi-quantitative analysis (Fig. 7M–N). Furthermore, RT-qPCR results shown in Fig. 7O–P demonstrated that OD/CS-PL@EVs group significantly upregulated the gene expression of *Col II*, *Acan* and *Sox-9* in both SMSCs and MCs, while OD/CS-PL group did not exhibit a significant upregulation trend in the expression of *Col II*, *Acan* and *Sox-9* in both SMSCs and MCs compared to the control group. These results together indicated that OD/CS-PL@EVs effectively promote the chondrogenic differentiation of SMSCs and the expression of cartilaginous extracellular matrix in MCs.

### 3.8. Response of macrophage to OD/CS-PL@EVs hydrogel adhesive

We then assessed the ability of OD/CS-PL@EVs hydrogel adhesive to regulate macrophage polarization *in vitro*. As indicated in Fig. 8A and C, the control group showed low fluorescence intensity of CCR7 and Arg-1, while the M0 macrophage treated with only stimulating factors group exhibited the highest fluorescence intensity of CCR7 and lowest intensity of Arg-1 at 72 h. Notably, the fluorescence intensity of CCR7 in the SF + OD/CS-PL@EVs group significantly decreased, while the intensity of Arg-1 markedly increased compared to the SF group. However, the fluorescence intensity of CCR7 and Arg-1 in the SF + OD/CS-PL group did not differ significantly compared to the SF group. Furthermore, Semi-quantitative analysis of the fluorescence intensity also demonstrated similar results (Fig. 8B–D). Next, flow cytometry exhibited that OD/CS-PL@EVs significantly reduced the ratio of CD86 and significantly increased the ratio of CD206 compared to the SF group (Fig. 8E–F). The results of MFI also yielded consistent conclusions (Fig. 8G–H). ELISA and RT-qPCR experiments demonstrated that OD/CS-PL@EVs significantly decreased the secretion and downregulated the gene expression of pro-inflammatory cytokines, while significantly increasing the secretion and upregulating the gene expression of anti-inflammatory cytokines. The expression of pro-inflammatory and anti-inflammatory cytokines in the OD/CS-PL group did not change significantly compared to the SF group (Fig. 8I–J). Therefore, OD/CS-PL@EVs possessed superior capability to inhibit the M1 polarization of macrophage and promote the M2 polarization.

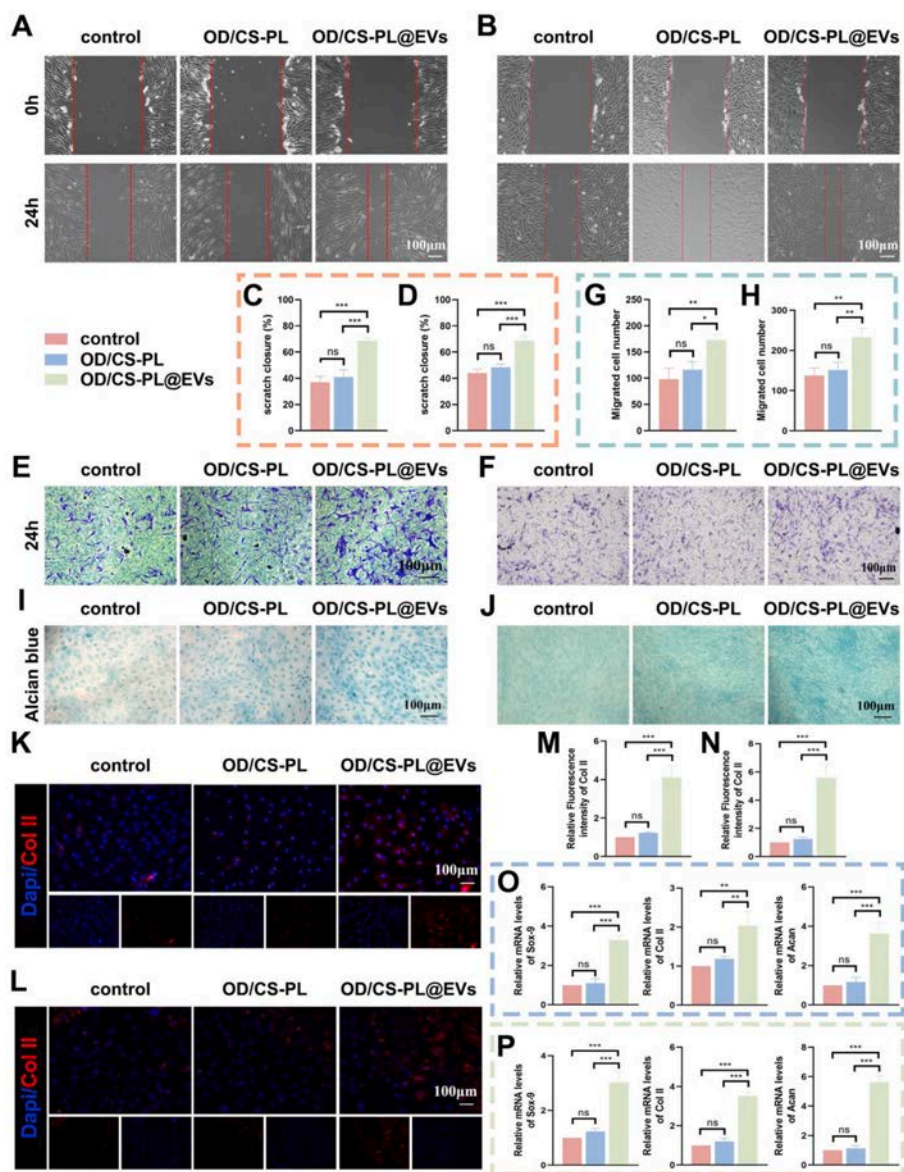


**Fig. 7.** The influence of OD/CS-PL@EVs hydrogel adhesive for SMSCs differentiation and ECM formation of MCs. A-B) Representative images of SMSCs and MCs migration under different treatments (PBS, OD/CS-PL and OD/CS-PL@EVs). C-D) Semi-quantitative analysis of SMSCs and MCs scratch assay, respectively. E-F) Representative images of SMSCs and MCs Transwell assay with different hydrogels in the down chamber. G-H) Semi-quantitative analysis of SMSCs and MCs Transwell assay, respectively. I-J) Representative images of SMSCs and MCs Alcian Blue staining. K-L) Representative immunofluorescence images of Col II expressed by SMSCs and MCs. M – N) Relative fluorescence intensity of Col II expressed by SMSCs and MCs, respectively. O-T) The mRNA expression of chondrogenic genes in SMSCs and MCs measured by RT-qPCR. Scale bar = 100  $\mu$ m ns represents no significance. \* $p$  < 0.05, \*\* $p$  < 0.01, \*\*\* $p$  < 0.001.

### 3.9. The immunoregulatory meniscus cartilage regeneration by OD/CS-PL@EVs hydrogel adhesive in meniscal defect model

Cylindrical defects on the anterior horn of the medial meniscus were created as the meniscus injury model (Fig. 9A–B). We then harvested the meniscus from the control, OD/CS-PL, OD/CS-PL@EVs, and the sham groups one week after surgery, prepared paraffin sections of the defect site, and performed immunofluorescent staining for TNF- $\alpha$  and IL-10 to evaluate the inflammatory status of the meniscus *in vivo*. The control group showed significantly high fluorescent intensity for TNF- $\alpha$  and low fluorescent intensity for IL-10, indicating the presence of an acute inflammatory response after meniscus injury. OD/CS-PL exhibited a slight decrease in TNF- $\alpha$  fluorescent intensity and a slight increase in IL-10 fluorescent intensity, while OD/CS-PL@EVs showed a significant decrease in TNF- $\alpha$  fluorescent intensity and a significant increase in IL-10 fluorescent intensity (Figs. S7A–B). The semi-quantitative analysis of

the fluorescence intensity of TNF- $\alpha$  and IL-10 similarly confirmed consistent results (Fig. S8). These results indicated that OD/CS-PL@EVs had superior immunomodulatory capability *in vivo*, regulating immune-microenvironment towards a favorable tissue regeneration status.

We further observed the macroscopic appearance of regenerated menisci in each group at weeks 6 and 12 postoperatively. No instances of knee joint infection or stiffness were found at 6 and 12 weeks. At week 6 postoperatively, there was no obvious repair observed in the meniscal defect area in the control group, while partial repair of the meniscus was observed in the OD/CS-PL group and OD/CS-PL@EVs group (Fig. 9C). At week 12, the meniscal defect area in the OD/CS-PL group and OD/CS-PL@EVs group showed further healing compared to the control group, while the control group did not exhibit obvious healing. It was worth noting that the meniscus of OD/CS-PL@EVs group showed a smooth surface, achieving the better healing effect compared to OD/CS-PL and the control group, although slightly weaker than the sham group

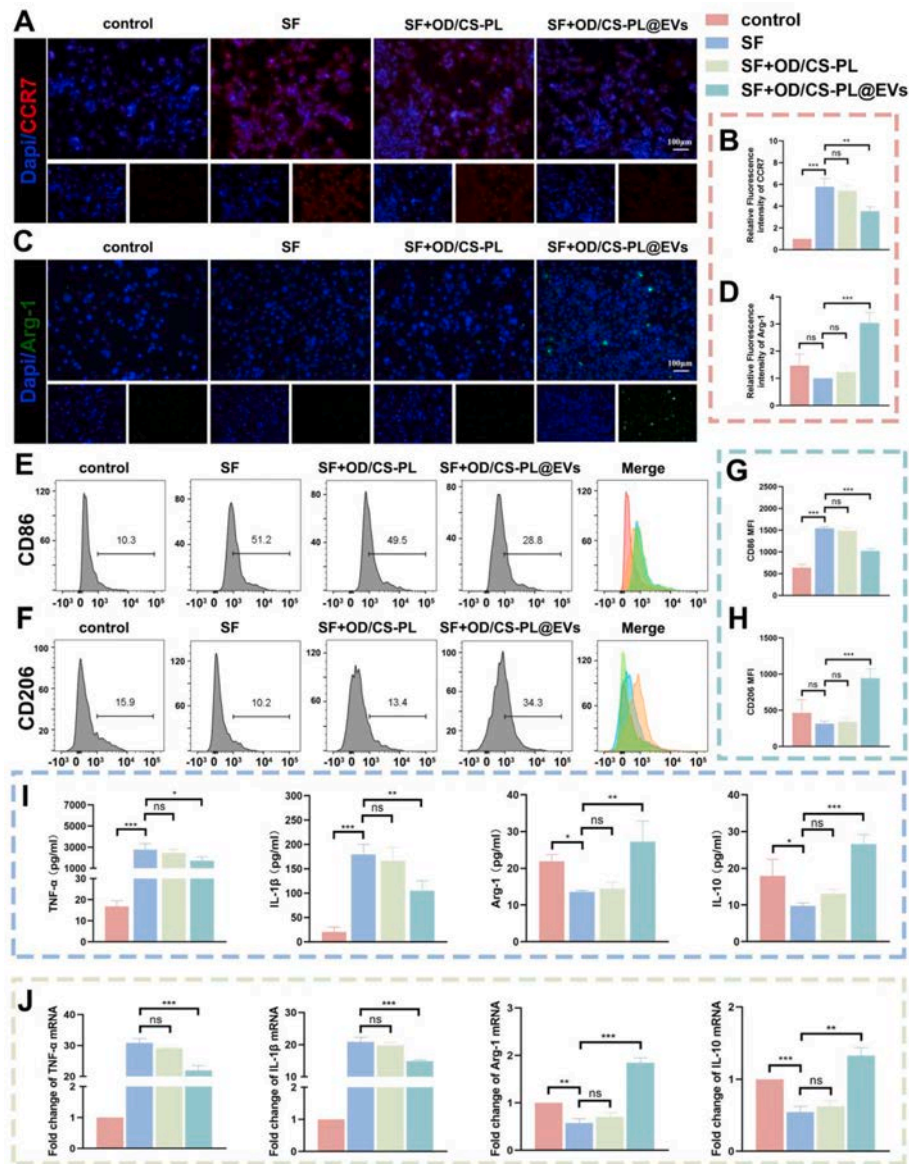


**Fig. 8.** OD/CS-PL@EVs hydrogel adhesive modulated the polarization of macrophages. A-B) Representative immunofluorescence images and relative fluorescence intensity of CCR7 (red) expressed by macrophages under different treatments (PBS, OD/CS-PL and OD/CS-PL@EVs). C-D) Representative immunofluorescence images and relative fluorescence intensity of Arg-1 (green) expressed by macrophages. E-F) Representative flow cytometry of macrophage markers CD86 (M1) and CD206 (M2). G-H) Mean fluorescence intensity of CD86 and CD206 measured by flow cytometry. I) The inflammatory cytokines expression of macrophage measured by ELISA. J) The mRNA expression of inflammatory genes measured by RT-qPCR. Scale bar = 100  $\mu$ m ns represents no significance. \* $p < 0.05$ , \*\* $p < 0.01$ , \*\*\* $p < 0.001$ . “SF” represents stimulating factors (100 ng/mL LPS and 20 ng/mL IFN- $\gamma$ ).

(Fig. 9D). The meniscus in the sham group were intact, as shown in Fig. S9.

The representative histological sections of regenerated menisci in each group are shown in Fig. 9E-L. As indicated in Fig. 9E and G at week 6, H&E, safranin O (S-O) histological staining results revealed severe loss and interruption of the menisci with no safranin O–stained matrix (red) in the control group at the defect site. In the OD/CS-PL group, the central area of the meniscus defect was filled with some regenerated tissue. Additionally, the menisci in the sham group appeared intact, and the inner and outer structures exhibited heterogeneity, with the inner structure consisting of numerous chondrocyte-like cells (Fig. S9). Notably, OD/CS-PL@EVs group displayed a greater amount of menisci tissue regeneration in the defect area with safranin O–stained matrix in the central defect site, and the regenerative tissue showed a predominance of round to oval-shaped chondrocyte-like morphology, which was similar with the inner area of the sham group. Furthermore, toluidine

blue (TB) staining results also showed that the OD/CS-PL@EVs group exhibited TB staining positive in the central of defect area compared with the control group and OD/CS-PL group (Fig. 9I). At week 12, the control group showed more regenerated menisci tissue compared to week 6, however, there was still a large area of interruption and loss in the defect area. The defect in the OD/CS-PL group was filled with irregularly regenerated menisci tissue, with some cells presenting chondrocyte-like characteristics. Interestingly, in the OD/CS-PL@EVs group, the meniscus defect was filled with regenerated tissue, and the new menisci tissue was firmly integrated with the defect edge, containing abundant chondrocyte-like cells as well as extracellular matrix (Fig. 9F). In addition, S-O staining (Fig. 9H) showed that the OD/CS-PL@EVs group exhibited strong positive staining for regenerated meniscal tissue, similar to the sham group, indicating a large amount of glycosaminoglycan in the extracellular matrix. In contrast, the control group exhibited relatively weak S-O staining, suggesting only a small

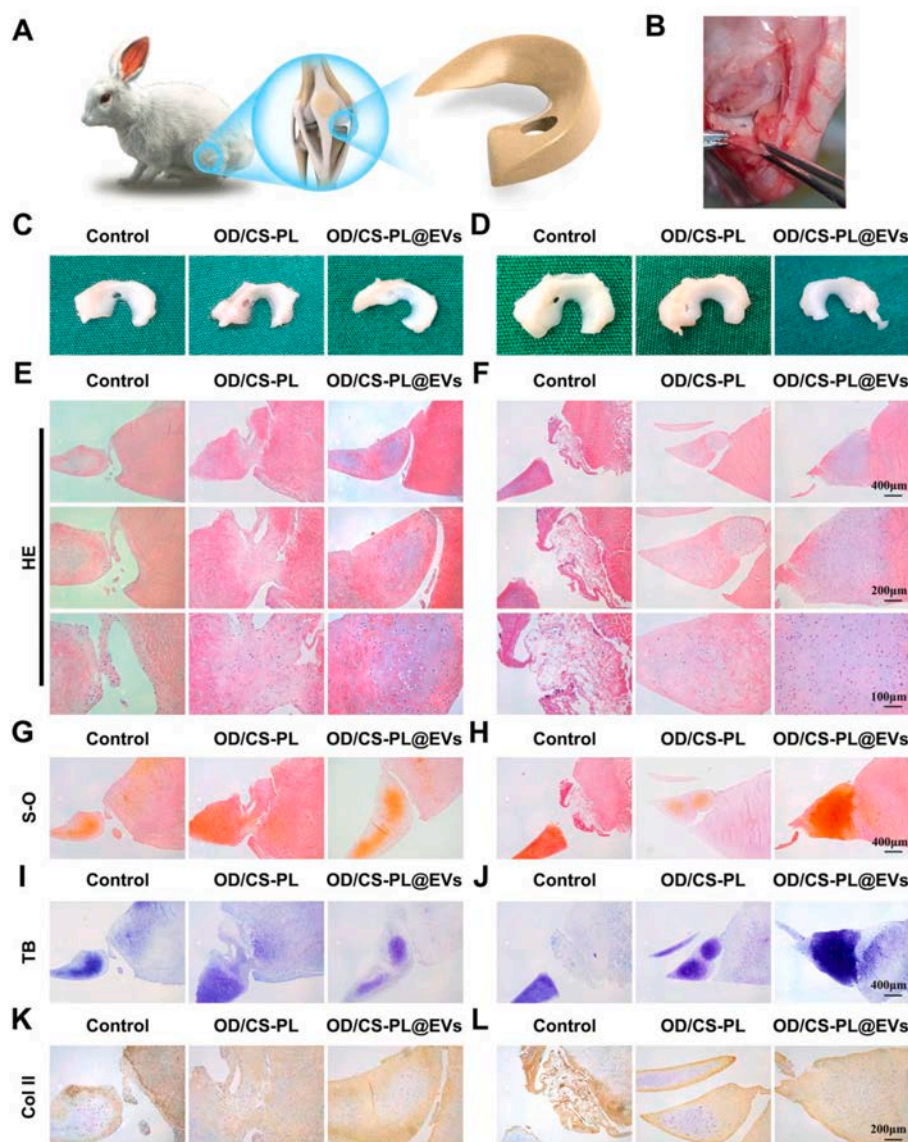


**Fig. 9.** Meniscal regeneration after implanting OD/CS-PL@EVs hydrogel adhesive. A) Schematic illustration of the construction of the meniscal defect model. B) Macroscopic appearance of meniscal cylindrical defect. C-D) Macroscopic observations of medial meniscus after surgery at weeks 6 and 12, respectively. E-F) Representative Hematoxylin and eosin (H&E) staining of meniscal tissue with different magnification in the different groups at weeks 6 and 12, respectively. Scale bar = 400  $\mu\text{m}$ , 200  $\mu\text{m}$ , or 100  $\mu\text{m}$ . G-H) Representative Safranin O (S-O) staining of meniscal tissue at weeks 6 and 12, respectively. Scale bar = 400  $\mu\text{m}$ . I-J) Representative Toluidine Blue (TB) staining of meniscal tissue at weeks 6 and 12, respectively. Scale bar = 400  $\mu\text{m}$ . K-L) Representative Col II staining of meniscal tissue at weeks 6 and 12, respectively. Scale bar = 200  $\mu\text{m}$ .

amount of glycosaminoglycan. S-O staining in the OD/CS-PL group was weaker than that in the OD/CS-PL@EVs group. Moreover, the OD/CS-PL@EVs group showed strong positive TB staining, similar to the medial area of the sham group.

Immunohistochemical analysis for Col II was also used to investigate the composition of the regenerated meniscal extracellular matrix. Considering that the inner avascular zone of the menisci is primarily composed of collagen II, collagen II staining was performed on each group, with the results shown in Fig. 9K-L. At week 6, Col II staining in the OD/CS-PL group and OD/CS-PL@EVs group was stronger than that in the control group, but weaker than that in the sham group. This result was also confirmed in the semi-quantitative analysis of Col II (Fig. S10). At week 12, Col II staining in the regenerated menisci of the OD/CS-PL@EVs group significantly intensified, indicating a substantial production of Col II at the injury site. Meanwhile, the new tissue in the OD/CS-PL group contained less Col II, and the control group even less. The trend of change was consistent with the semi-quantitative analysis of Col

II (Fig. S10).

### 3.10. Delay of articular cartilage degeneration by OD/CS-PL@EVs hydrogel adhesive

We assessed the protective effect of OD/CS-PL@EVs hydrogel adhesive on articular cartilage. The medial femoral condyle (FC) and tibial plateau (TP) were harvested, and International Cartilage Repair Society (ICRS) cartilage lesions classification was used for macroscopic evaluation, as shown in Fig. 10A-D, and E, the control group showed the highest ICRS scores at both weeks 6 and 12. However, the ICRS scores were found to be no statistically significant difference between the OD/CS-PL group, OD/CS-PL@EVs group, and the sham group at weeks 6 and 12. Histological evaluation revealed partial disintegration of the cartilage in FC and TP of the control group, with decrease in TB staining intensity at week 6. Moreover, at week 12, the control group showed more severe cartilage damage over time. The surfaces of the cartilage in

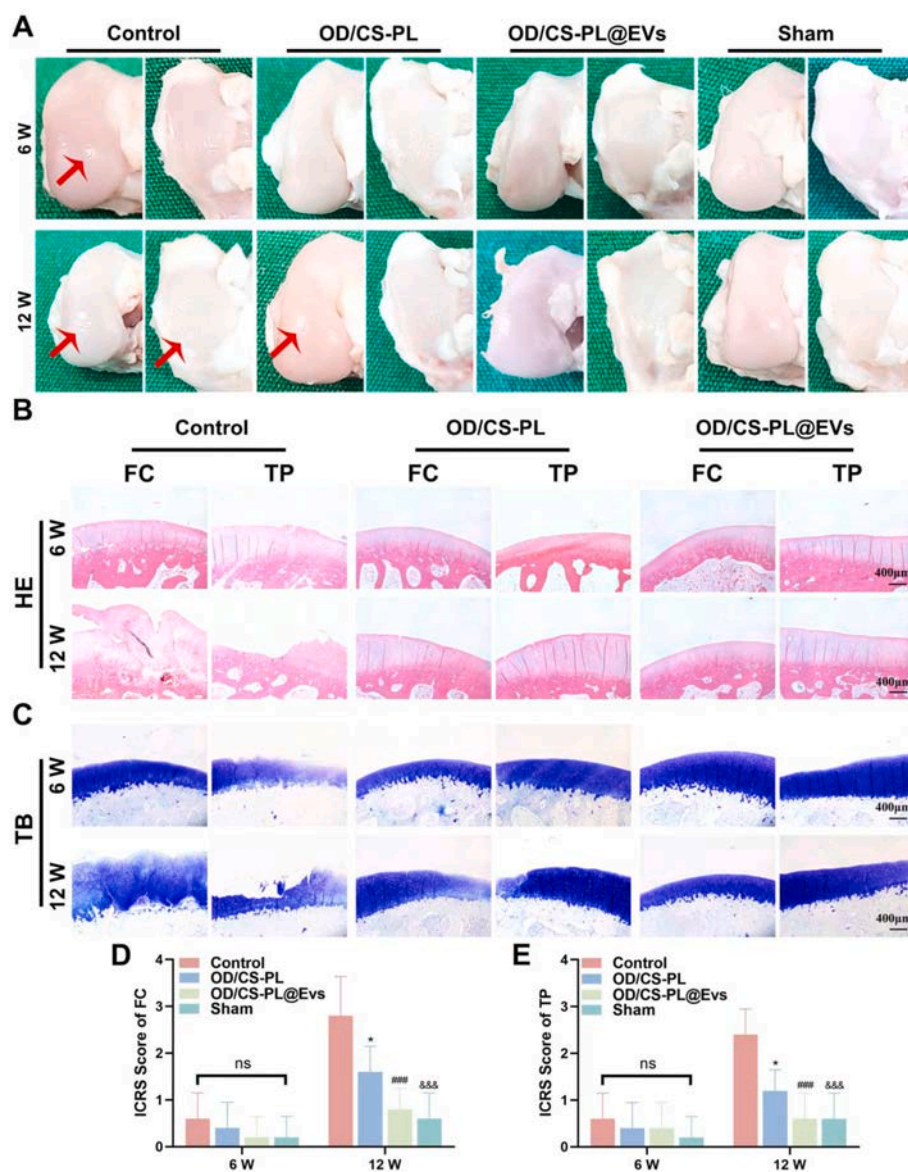


**Fig. 10.** Effect of articular cartilage protection of OD/CS-PL@EVs hydrogel adhesive at weeks 6 and 12. A) Macroscopic appearance of the tibial plateau (TP) and femoral condyle (FC) in the different groups at weeks 6 and 12, respectively. B–C) Representative H&E and TB staining of cartilage surfaces in the TP and FC. Scale bar = 400  $\mu$ m. D–E) Cartilage degeneration of TP and FC evaluated using ICRS scores. ns represents no significance. \* $p < 0.05$ , when compared with the control group. ### $p < 0.001$ , when compared with control group. &&& $p < 0.001$ , when compared with the control group. Red arrows indicate obvious cartilage damage.

the OD/CS-PL group exhibited roughness or decreased TB staining intensity, whereas the surfaces of the cartilage in the OD/CS-PL@EVs group and the sham group showed similar conditions with no apparent damage (Fig. 10B–C and S11). Together, OD/CS-PL@EVs hydrogel adhesive protected the articular cartilage from the progressive degeneration after meniscus injury.

### 3.11. OD/CS-PL@EVs hydrogel adhesive promotes meniscus reconstruction with enhanced biomechanical strength

At week 12, the mechanical test was conducted on the regenerated meniscus tissue in each group. The OD/CS-PL@EVs group exhibited a significantly higher compressive stress in the regenerated tissue compared to both the control group and the OD/CS-PL group, and showed no significant difference compared to the sham group in terms of compressive stress (Fig. S12).

### 3.12. Systemic biosafety analysis of OD/CS-PL@EVs hydrogel adhesive

Finally, H&E staining of the main organs (heart, liver, kidney, lung, and spleen) in all groups were analyzed at week 12. As shown in Fig. S13, the results showed no significant adverse reactions from the implantation of OD/CS-PL and OD/CS-PL@EVs groups. Therefore, the implantation of OD/CS-PL@EVs hydrogel adhesive was considered to be biologically safe.

## 4. Discussion

In this study, we designed and prepared a highly wet-adhesive antibacterial hydrogel, and loaded it with SMSCs-derived EVs to create a convenient injectable hydrogel system, aiming to achieve effective adhesion to the injured meniscus and prevent microbial invasion in the wet intra-articular microenvironment. This hydrogel system also exhibited the capability to regulate immune homeostasis, mobilize the proliferation and recruitment capacity of endogenous cells,

stimulate the chondrogenic differentiation of stem cells, and promote cell ingrowth into the hydrogel, thereby achieving the regeneration of meniscal cartilaginous tissue *in vivo*, which presented a promising treatment strategy for meniscus repair.

A novel wet-adhesive glycopeptide OD/CS-PL hydrogel adhesive was fabricated and demonstrated excellent adhesion to wet tissues, including the meniscus, with the adhesion strength reached  $134.45 \pm 28.69$  KPa in this work. Previous studies have also documented the mechanical properties of hydrogel adhesion to meniscus and cartilage surfaces. For example, a double-network hydrogel was reported to exhibit adhesion to the cartilage surface, achieving the adhesion strength of 130 KPa, which was superior to commercially adhesive hydrogels [45]. In addition, a mussel-inspired adhesive hydrogel was demonstrated to achieve a shear strength of 120 KPa [37]. Therefore, the adhesion mechanics of OD/CS-PL and OD/CS-PL@EVs hydrogel adhesives meet the mechanical requirements reported for meniscus repair [17]. Notably, all components of this composite glycopeptide hydrogel are FDA-approved substances (dextran, CS, and PL) with excellent biocompatibility, holding promising potential for clinical translation. Dextran could be oxidized to the aldehyde group to prepare OD, which could attach to the tissue surface or prepare the hydrogel via the formation of Schiff base bonds. CS with the amino and carboxyl groups was frequently conjugated oxidized dextran to prepare qualified adhesion OD/CS cross-linked network structure to apply in the biomedical field [24]. Additionally, PL with intrinsic non-antigenicity, antibacterial properties, biocompatibility, and biodegradability, as well as possessing free amines on the side chain, which displayed profound bioactivity and multi-function in various biomedical applications [27]. PL effectively enhanced the mechanical strength and adhesion performance of the OD/CS hydrogel. The existence  $-COOH$  of CS, could crosslink with PL by the amide reaction under mild conditions, while the  $-CHO$  of OD crosslinks with the  $-NH_2$  of PL and CS by the Schiff base reaction to form OD/CS-PL hydrogel adhesive. This hydrogel provided an effective delivery vehicle for the regeneration of injured meniscal tissue. In addition, by simply mixing OD-PL and CS using a double-barreled syringe, the OD/CS-PL hydrogel adhesive could be prepared at room temperature effectively and practically. Furthermore, this gelation approach offers more merits compared to the UV-curing approach, as the limited availability and penetration depth of the latter restricts its use in joint spaces [23]. Previous studies have reported the development of synthetic scaffolds for meniscal regeneration. However, such substitutes often cannot integrate well with the host meniscus and require extensive trimming of the host meniscus for fixation, inevitably resulting in additional loss of meniscal tissue [4]. The OD/CS-PL hydrogel adhesive significantly reduces the operational difficulty of the hydrogel in clinical practice, allowing it to be easily squeezed and applied to the damaged meniscus with a syringe for adhesion. This operational process effectively achieves the maximum protection of the host meniscus integrity and demonstrates significant benefits in meniscus regeneration, considering the advantageous delivery strategies of irregular tissues in the wet environment. Additionally, hydrogels with a porous structure play a crucial role in regulating tissue regeneration processes, such as cell infiltration, migration, and extracellular matrix deposition. Compared to nano-sized pores, hydrogels with micro-sized pores could be better at promoting nutrient transport and metabolite release, potentially accelerating the degradation of hydrogel, and promoting tissue repair [46]. The OD/CS-PL hydrogel adhesive exhibited a microporous structure with a pore size of  $47.8 \pm 13.6$   $\mu\text{m}$ , which remained unchanged after loading EVs. The OD/CS-PL@EVs hydrogel adhesive effectively accelerated the degradation of the hydrogel subcutaneously and facilitated cell infiltration. This contributes to the hydrogel being rapidly replaced by cells and new tissue during the tissue repair process, enabling the hydrogel to integrate with the host tissue as soon as possible.

EVs from SMSCs were selected and loaded onto OD/CS-PL@EVs hydrogel adhesive to exhibit biological effects in this study. The results indicated that EVs demonstrated a promoting effect on endogenous

cells (SMSCs and MCs), including their proliferation, recruitment, chondrogenic differentiation, and ECM formation abilities. These results were consistent with existing research findings [31,32]. Although various stem cells-derived extracellular vesicles were reported to promote tissue healing, currently only SMSCs-EVs was investigated for their role in meniscus regeneration, and their research findings indicate that EVs might promote meniscus repair by mediating endogenous cell proliferation and migration through the CXCL5 and CXCL6/CXCR2 axis, which can enhance stem cell growth and migration during tissue healing [31]. However, in the *in vivo* experiments of these studies, EVs were only directly injected into the joint cavity. Although the reported results were promising, the transient release of EVs might prevent long-term effectiveness in cartilage and meniscal regeneration processes. Furthermore, when loaded into OD/CS-PL@EVs hydrogel adhesive, the hydrogel adhesive exhibited similar regulatory capabilities over endogenous cells *in vitro* and achieved substantial cell infiltration as well as regeneration of cartilage-like tissue at the site of meniscal defects in rabbits. The meniscus, as a heterogeneous fibrocartilage, differs in composition and function between its inner and outer zones. The inner zone, characterized by a lack of blood supply, primarily consists of chondrocytes and bears compressive loads [43]. Therefore, for repairs in avascular regions, it is essential to reconstruct the natural inner zone tissue structure. The OD/CS-PL@EVs hydrogel adhesive effectively restored the avascular cartilage-like tissue of the meniscus, thereby potentially restoring the original function. The poor healing of the meniscal avascular area has always been a clinical challenge. After meniscal injury, multiple factors influence meniscal avascular zone repair, especially inadequate cell recruitment and inflammatory response [3]. Recently, to overcome the characteristic of low endogenous cell recruitment ability, current studies reported that various types of stem cells directly applied for meniscal injury repair, either alone or with the assistance of a scaffold [47]. Among these, SMSCs, which are considered an endogenous stem cell source for meniscal repair, might be a preferred option for stem cell therapy [28]. Furthermore, the acquisition of SMSCs is relatively minimally invasive, as they can be obtained through simple arthroscopic surgery, and requires minimal tissue demand [47]. However, cell-based therapeutic strategies typically have some inherent drawbacks as mentioned above. Considering that stem cell-mediated tissue regeneration primarily involves activating resident cells through paracrine mechanisms, EVs from stem cell paracrine secretion, with low antigenicity and relative controllability, have been extensively documented to exert beneficial effects on cellular functions [30]. Additionally, the primary goal of meniscus repair is to delay the progression of osteoarthritis, and SMSCs-EVs was reported to play a crucial role in protecting articular cartilage. Therefore, in this study, SMSCs-EVs released from adhesives may also directly contribute to protecting articular cartilage [48]. Therefore, by constructing the OD/CS-PL@EVs hydrogel adhesive, it was endowed with the ability to efficiently regulate the endogenous regenerative cell behaviors, adequately addressing the drawback of insufficient endogenous cells during meniscal regeneration process. Chen et al. constructed the GelMA-Aptamer system to recruit synovial cells and meniscus cells, demonstrating promising meniscus regeneration at week 12, similar to this study's findings in delaying cartilage degeneration. However, this system lacks adhesive properties, potentially posing a risk of hydrogel detachment [9]. Pan et al. prepared TGF- $\beta$ 1 loaded silk fibroin hydrogel adhesive for meniscus injury repair, exhibiting good wet adhesion and anti-swelling properties. The adhesive was reported to achieve meniscus repair. While it needs to be considered that there are issues regarding the singular biological effect and safety of growth factors [5,49].

This study indicated that the EVs derived from SMSCs could regulate the inflammatory state of macrophages induced by THP-1. EVs exhibited significant inhibitory effects on the transformation of macrophages to the M1 phenotype and the polarization towards the M2 phenotype. In addition, the OD/CS-PL@EVs hydrogel adhesive also demonstrated consistent immunomodulatory effects. Furthermore, the inflammatory

markers of meniscal defects were assessed in rabbits at one-week post-surgery. The damaged meniscus intervened with the OD/CS-PL@EVs hydrogel adhesive demonstrating a significant increase in IL-10 and a decrease in TNF- $\alpha$ . Combined with *in vitro* results, this anti-inflammatory effect is mainly attributed to the addition of EVs in the hydrogel. Therefore, the superior anti-inflammatory performance of the OD/CS-PL@EVs hydrogel adhesive was effective in regulating the immune microenvironment of damaged meniscus. In addition to the limitation of inadequate endogenous cells, it was reported that the pro-inflammatory markers were significantly upregulated following meniscal injury and exerted an inhibitory effect on the meniscal cartilage regeneration [3]. Multiple immune cells participate in cartilage injury and repair, including macrophages, T cells, natural killer (NK), etc., among which macrophages playing a crucial role during the repair phase. Macrophages are mainly categorized into M1 and M2 phenotypes, where M1 macrophages lead to cartilage degradation, while M2 macrophages promote the resolution of inflammation and chondrogenic differentiation of MSCs [33]. Therefore, effectively intervening with macrophages and inducing their transition to the M2 phenotype will create favorable conditions for meniscal cartilage tissue regeneration [34]. Although the application of EVs for regulating the treatment of tissue injury-related diseases has been widely reported, it is noteworthy that this study represented the attempt to utilize EVs to intervene in the immune homeostasis regulation after meniscus injury, and achieved exciting results. Meanwhile, current studies on regulating the meniscal inflammation environment only achieved a single anti-inflammatory effect, often required the addition of other biological agents to achieve regenerative purposes, making the preparation process of tissue engineering scaffolds more complex and difficult to control [34]. This study, by loading a single EVs component, enabled the hydrogel to simultaneously achieve immune homeostasis and regulate endogenous cell behavior, ensuring the stability and convenience of hydrogel fabrication. Although antagonists of pro-inflammatory cytokines were reported to promote meniscal tissue repair within an inflammatory microenvironment *in vitro* [50]. Currently available anti-inflammatory drugs used in clinical practice, such as non-steroidal anti-inflammatory drugs, are typically aimed at symptom relief instead of preventing or reducing inflammatory reactions. Therefore, based on the tremendous potential demonstrated by EVs in meniscus injury repair, they are expected to replace or enhance existing anti-inflammatory drugs as bioactive agents. In addition, RNA sequencing was further used to reveal the mechanisms by which EVs inhibit inflammation and promote macrophage polarization toward the M2 phenotype in this study. EVs significantly down-regulated the signaling pathways (cytokine-cytokine receptor interaction, chemokine signaling pathway and toll-like receptor signaling pathway, and NOD-like receptor pathway) associated with inflammation when macrophages were co-cultured with stimulating factors and EVs, and previous studies reported that different treatment strategies achieved effective inflammation regulation by inhibiting these inflammation-related pathways [46,51,52]. However, this study did not further investigate the specific substances in EVs that regulated inflammatory responses, such as proteins and miRNAs, which require additional exploration in future research.

In this work, CS, as chitosan-modified derivative rich in amino groups, retains the inherent antibacterial properties and biocompatibility, which could be reflected in the fact that both prepared OD/CS and OD/CS@EVs hydrogels exhibit certain antibacterial effects against the two types of bacteria. Furthermore, the introduction of antibacterial peptide (PL) further contributed to the excellent antibacterial performance of the OD/CS-PL and OD/CS-PL@EVs hydrogel adhesives, both of which exhibited superior antibacterial ability against two clinically common bacteria within only 12 h of intervention. In addition to sterile inflammation, implant infection also deserves attention when implanting foreign grafts in human body. It has always been one of the most challenging issues in orthopedic clinical practice, posing a serious threat to human health and causing significant economic losses. Additionally,

even if the presence of microorganisms does not lead to extreme infectious events, it can still activate the body's immune system, subsequently triggering a series of inflammatory responses, which severely disrupt the tissue repair process [25]. Unfortunately, most tissue engineering scaffolds did not simultaneously possess antibacterial ability [6]. Therefore, it is essential to design implants with effective antibacterial properties to ensure that cells and tissues are in a safe environment. In addition, the commonly used anti-infection strategies involve the administration of metal nanoparticles or antibiotics either systemically or locally. While these treatments often result in the emergence of multidrug-resistant bacteria [53]. Metal nanoparticles might have limitations in terms of biodegradability and cellular compatibility and potentially trigger adverse effects on the immune system [54]. In this study, PL is the key component in the hydrogel system responsible for antibacterial activity. It is a natural antibacterial peptide with cationic characteristics that allow it to interact directly with anionic bacterial membranes. Through its amphipathic structure, it disrupts the cell membrane, leading to antibacterial effects. Additionally, it can also target bacterial proteins and nucleic acids, inhibiting bacterial growth. Compared to antibiotics, antibacterial peptides act through a non-receptor-mediated mechanism to irreversibly disrupt bacterial membranes. This makes it difficult for bacteria to develop resistance, making antibacterial peptides one of the most promising antibacterial agents in addressing antibiotic resistance challenges [55]. Therefore, the OD/CS-PL@EVs hydrogel adhesive not only achieved superior antibacterial performance but also maintained good biocompatibility and enhanced its own wet-adhesive properties.

The goal of achieving biomimetic repair of the meniscal avascular zone structure is to restore the compressive mechanical properties of meniscus tissue and reshape its protective role in the knee joint [1]. Therefore, this study investigated the protective effects of meniscus on articular cartilage in different groups. The results showed that the OD/CS-PL@EVs group achieved the best cartilage protection effect, which was also confirmed by scoring analysis. Furthermore, this study also conducted compression mechanical testing on the regenerated meniscal tissue and found that the OD/CS-PL@EVs group exhibited superior compression mechanical values among the different groups. These indicated that through the intervention of OD/CS-PL@EVs hydrogel adhesive, the damaged meniscus achieved good histological and mechanical functional recovery. In future clinical applications, the OD/CS-PL@EVs hydrogel adhesive, as a promising method, are expected to be directly applied to *in situ* repair of meniscal tears. Additionally, it can be combined with meniscus suture techniques for use on larger areas of meniscal tears, contributing to biologically enhanced repair. In this study, the OD/CS-PL@EVs hydrogel adhesive consists of components approved by FDA, which facilitates clinical translation. In addition, the low immunogenicity of EVs also provide a certain guarantee for clinical safety. The injectable form of adhesive also simplifies the steps of intraoperative procedures, making it convenient for clinical applications. Future work will further explore the exact mechanisms by which EVs regulate immunity and promote meniscal regeneration, providing a solid theoretical basis for clinical translation. Additionally, the animal model will shift to large animals, such as ovine and pigs, whose menisci are physiologically more similar to the human meniscus. Furthermore, there will be some preclinical research conducted to evaluate the biosafety of the adhesive.

## 5. Conclusion

This study represents the report of a versatile bio-enhanced hydrogel employed in meniscus repair, offering high wet adhesion, effective antibacterial properties, and providing superior immunomodulatory effects and enhanced meniscal cartilage regeneration capabilities through SMSCs-EVs loading. The hydrogel can be effectively adhered to the irregular and wet surface of the meniscus by squeezing it with a syringe easily. The microporous structure facilitates cell infiltration and

tissue regeneration, and its broad-spectrum antibacterial properties ensure the prevention of implant infection. The released EVs exhibit sequential therapeutic function, regulating the inflammatory microenvironment at the site of meniscal injury by reducing the expression of multiple inflammation-related signaling pathways, promoting endogenous cell proliferation, migration, and cartilaginous matrix formation. In a rabbit meniscal defect model, the hydrogel facilitates cartilage regeneration in the meniscal avascular zone and enhances the biomechanical strength of the regenerated meniscal tissue, delaying the degeneration of articular cartilage. The simple and effective hydrogel preparation method developed in this study, with its versatile biological functions, holds promise as a potential means for clinically treating meniscal avascular zone injuries.

### CRedit authorship contribution statement

**Moran Huang:** Writing – original draft, Investigation, Data curation, Conceptualization. **Zhengchao Yuan:** Writing – original draft, Data curation, Conceptualization. **Guojian Fu:** Writing – review & editing, Investigation. **Jize Dong:** Software, Methodology, Investigation. **Yaying Sun:** Investigation. **Wenxin Wang:** Software. **Muhammad Shafiq:** Software. **Huiliang Cao:** Writing – review & editing. **Xiumei Mo:** Writing – review & editing, Funding acquisition, Conceptualization. **Jiwu Chen:** Writing – review & editing, Project administration, Funding acquisition, Conceptualization.

### Ethics approval and consent to participate

The isolation of human SMSCs was approved by the Ethics Committee of the Shanghai General Hospital (2022KY068C23-1).

The approval for all animal experiments was obtained from the Animal Welfare & Ethics Committee of the Shanghai General Hospital (2022AW032).

### Declaration of competing interest

The authors declare that they have no known competing financial interests or personal relationships that could have appeared to influence the work reported in this paper.

### Acknowledgement

This work was financially supported by the National Natural Science Foundation of China (Grant No. 82372491 and 82172509); the Science and Technology Commission of Shanghai Municipality, China (20DZ2254900).

### Appendix A. Supplementary data

Supplementary data to this article can be found online at <https://doi.org/10.1016/j.compositesb.2024.111970>.

### Data availability

Data will be made available on request.

### References

- [1] Makris EA, Hadidi P, Athanasiou KA. The knee meniscus: structure-function, pathophysiology, current repair techniques, and prospects for regeneration. *Biomaterials* 2011;32(30):7411–31.
- [2] Lombardo MDM, Mangiavini L, Peretti GM. Biomaterials and meniscal lesions: current concepts and future perspective. *Pharmaceutics* 2021;13(11).
- [3] Yan W, Dai W, Cheng J, Fan Y, Wu T, Zhao F, Ao Y. Advances in the mechanisms affecting meniscal avascular zone repair and therapies. *Front Cell Dev Biol* 2021;9:758217.
- [4] Noh S, Jin YJ, Shin DI, Kwon HJ, Yun HW, Kim KM, Park DY. Selective extracellular matrix guided mesenchymal stem cell self-aggregate engineering for replication of meniscal zonal tissue gradient in a porcine meniscectomy model. *Adv Healthcare Mater* 2023;12(27):e2301180.
- [5] Pan X, Li R, Li W, Sun W, Yan Y, Xiang X, Ouyang H. Silk fibroin hydrogel adhesive enables sealed-tight reconstruction of meniscus tears. *Nat Commun* 2024;15(1):2651.
- [6] Bandyopadhyay A, Ghibhela B, Mandal BB. Current advances in engineering meniscal tissues: insights into 3D printing, injectable hydrogels and physical stimulation based strategies. *Biofabrication* 2024;16(2).
- [7] Ran X, Wang Q, Sun Y, Pan Q, Chen H, Ren W, Wang X. Dual microparticles programmed delivery system regulating stem cell-based cartilage regeneration by cartilage-specific matrix hydrogels. *Compos B Eng* 2024;272:111221.
- [8] Xu Y, Wang J, Liu Z, Qiu H, Song L, Liu S, Zhang X. Cartilage regeneration achieved in photo-crosslinked hyaluronic hydrogel bioactivated by recombinant humanized collagen type III. *Compos B Eng* 2024;288:111886.
- [9] Chen Z, Deng XH, Jiang C, Wang JS, Li WP, Zhu KL, Zhang ZZ. Repairing avascular meniscal lesions by recruiting endogenous targeted cells through bispecific synovial-meniscal aptamers. *Am J Sports Med* 2023;51(5):1177–93.
- [10] Zhong G, Yao J, Huang X, Luo Y, Wang M, Han J, Yu Y. Injectable ECM hydrogel for delivery of BMSCs enabled full-thickness meniscus repair in an orthotopic rat model. *Bioact Mater* 2020;5(4):871–9.
- [11] Wang K, Zhang Y, Chen T, Bai L, Li H, Tan H, Qu X. Chain entanglement-driven tough, fatigue-resistant PEG-based injectable hydrogel adhesive for joint skin wound healing. *Compos B Eng* 2023;266:110991.
- [12] Lee S, Kang JI, Kim Y, Park KM. Oxygen-generating tissue adhesives via CaO<sub>2</sub>-mediated oxygen generation and in situ catechol oxidation for wound management. *Compos B Eng* 2023;266:110951.
- [13] Ma Z, Bao G, Li J. Multifaceted design and emerging applications of tissue adhesives. *Adv Mater* 2021;33(24):2007663.
- [14] Zöller K, To D, Bernkop-Schnürch A. Biomedical applications of functional hydrogels: innovative developments, relevant clinical trials and advanced products. *Biomaterials* 2024;312:122718.
- [15] Wei Y, Jin X, Luo Q, Li Q, Sun G. Adhesively bonded joints – a review on design, manufacturing, experiments, modeling and challenges. *Compos B Eng* 2024;276:111225.
- [16] Yang J, Bai R, Chen B, Suo Z. Hydrogel adhesion: a supramolecular synergy of chemistry, topology, and mechanics 2020;30(2):1901693.
- [17] Marom N, Ode G, Cox F, Jivanelli B, Rodeo SA. Current concepts on tissue adhesive use for meniscal repair—we are not there yet: a systematic review of the literature. *Am J Sports Med* 2022;50(5):1442–50.
- [18] Bochyńska AI, Hannink G, Verhoeven R, Grijpma DW, Buma P. Evaluation of novel biodegradable three-armed- and hyper-branched tissue adhesives in a meniscus explant model. *J Biomed Mater Res* 2017;105(5):1405–11.
- [19] Wong P-C, Chen K-H, Wang W-R, Chen C-Y, Wang Y-T, Lee Y-B, Wu J-L. Injectable ChitHCl-DDA tissue adhesive with high adhesive strength and biocompatibility for torn meniscus repair and regeneration. *Int J Biol Macromol* 2024;270:132409.
- [20] Cui C, Liu W. Recent advances in wet adhesives: adhesion mechanism, design principle and applications. *Prog Polym Sci* 2021;116:101388.
- [21] Gao W, Chen K, He W, Zhao S, Cui D, Tao C, Xia H. Synergistic chondrogenesis promotion and arthroscopic articular cartilage restoration via injectable dual-drug-loaded sulfated hyaluronic acid hydrogel for stem cell therapy. *Compos B Eng* 2023;263:110857.
- [22] Jayakumar R, Prabakaran M, Nair SV, Tokura S, Tamura H, Selvamurugan N. Novel carboxymethyl derivatives of chitin and chitosan materials and their biomedical applications. *Prog Mater Sci* 2010;55(7):675–709.
- [23] Chen Z, Zhao J, Wu H, Wang H, Lu X, Shahbazi MA, Wang S. A triple-network carboxymethyl chitosan-based hydrogel for hemostasis of incompressible bleeding on wet wound surfaces. *Carbohydr Polym* 2023;303:120434.
- [24] Balakrishnan B, Soman D, Payanam U, Laurent A, Labarre D, Jayakrishnan A. A novel injectable tissue adhesive based on oxidized dextran and chitosan. *Acta Biomater* 2017;53:343–54.
- [25] Wang Z, Yu Z, Wang Z, Li S, Song L, Xu T, Gao C. Surface-activated 3D-printed PEEK implant enhances anti-infection and osteogenesis. *Compos B Eng* 2024;273:111258.
- [26] Xi Y, Ge J, Guo Y, Lei B, Ma PX. Biomimetic elastomeric polypeptide-based nanofibrous matrix for overcoming multidrug-resistant bacteria and enhancing full-thickness wound healing/skin regeneration. *ACS Nano* 2018;12(11):10772–84.
- [27] Zhu H, Liu R, Shang Y, Sun L. Polylysine complexes and their biomedical applications. *Engineered Regeneration* 2023;4(1):20–7.
- [28] Kim W, Onodera T, Kondo E, Terkawi MA, Homan K, Hishimura R, Iwasaki N. Which contributes to meniscal repair, the synovium or the meniscus? An in vivo rabbit model study with the freeze-thaw method. *Am J Sports Med* 2020;48(6):1406–15.
- [29] Sekiya I, Koga H, Katano H, Mizuno M, Kohno Y, Otobe K, Ozeki N. Second-look arthroscopy after meniscus repair and synovial mesenchymal stem cell transplantation to treat degenerative flaps and radial tears of the medial meniscus: a case report. *J Orthop Sci : official journal of the Japanese Orthopaedic Association* 2022;27(4):821–34.
- [30] Ju Y, Hu Y, Yang P, Xie X, Fang B. Extracellular vesicle-loaded hydrogels for tissue repair and regeneration. *Materials today. Bio* 2023;18:100522.
- [31] Kawata K, Koga H, Tsuji K, Miyatake K, Nakagawa Y, Yokota T, Katagiri H. Extracellular vesicles derived from mesenchymal stromal cells mediate endogenous cell growth and migration via the CXCL5 and CXCL6/CXCR2 axes and repair meniscus. *Stem Cell Res Ther* 2021;12(1):414.
- [32] Li Q, Yu H, Sun M, Yang P, Hu X, Ao Y, Cheng J. The tissue origin effect of extracellular vesicles on cartilage and bone regeneration. *Acta Biomater* 2021;125:253–66.

- [33] Li M, Yin H, Yan Z, Li H, Wu J, Wang Y, Guo Q. The immune microenvironment in cartilage injury and repair. *Acta Biomater* 2022;140:23–42.
- [34] Xu B, Ye J, Fan BS, Wang X, Zhang JY, Song S, Yu JK. Protein-spatiotemporal partition releasing gradient porous scaffolds and anti-inflammatory and antioxidant regulation remodel tissue engineered anisotropic meniscus. *Bioact Mater* 2023;20:194–207.
- [35] Clair AJ, Kingery MT, Anil U, Kenny L, Kirsch T, Strauss EJ. Alterations in synovial fluid biomarker levels in knees with meniscal injury as compared with asymptomatic contralateral knees. *Am J Sports Med* 2019;47(4):847–56.
- [36] Huang L, Zhang S, Wu J, Guo B, Gao T, Shah SZA, Chen H. Immunity-and-matrix-regulatory cells enhance cartilage regeneration for meniscus injuries: a phase I dose-escalation trial. *Signal Transduct Targeted Ther* 2023;8(1):417.
- [37] Zhang F-X, Liu P, Ding W, Meng Q-B, Su D-H, Zhang Q-C, Jiang L-B. Injectable Mussel-Inspired highly adhesive hydrogel with exosomes for endogenous cell recruitment and cartilage defect regeneration. *Biomaterials* 2021;278:121169.
- [38] Amemiya M, Tsuji K, Katagiri H, Miyatake K, Nakagawa Y, Sekiya I, Koga H. Synovial fluid-derived mesenchymal cells have non-inferior chondrogenic potential and can be utilized for regenerative therapy as substitute for synovium-derived cells. *Biochem Biophys Res Commun* 2020;523(2):465–72.
- [39] Wang L, Wu Y, Tan Y, Fei X, Deng Y, Cao H, Chen L. Cytotoxic effects of the quinolone levofloxacin on rabbit meniscus cells. *J Appl Toxicol : J Anal Toxicol* 2014;34(8):870–7.
- [40] Théry C, Witwer KW, Aikawa E, Alcaraz MJ, Anderson JD, Andriantsitohaina R, Zuba-Surma EK. Minimal information for studies of extracellular vesicles 2018 (MISEV2018): a position statement of the International Society for Extracellular Vesicles and update of the MISEV2014 guidelines. *J Extracell Vesicles* 2018;7(1):1535750.
- [41] Daigneault M, Preston JA, Marriott HM, Whyte MK, Dockrell DH. The identification of markers of macrophage differentiation in PMA-stimulated THP-1 cells and monocyte-derived macrophages. *PLoS One* 2010;5(1):e8668.
- [42] Brittberg M, Winalski CS. Evaluation of cartilage injuries and repair. *J Bone Joint Surg Am* 2003;85(A Suppl 2):58–69.
- [43] Zhang ZZ, Chen YR, Wang SJ, Zhao F, Wang XG, Yang F, Jiang D. Orchestrated biomechanical, structural, and biochemical stimuli for engineering anisotropic meniscus. *Sci Transl Med* 2019;11(487).
- [44] Mankin HJ, Dorfman H, Lippicello L, Zarins A. Biochemical and metabolic abnormalities in articular cartilage from osteo-arthritic human hips. II. Correlation of morphology with biochemical and metabolic data. *J Bone Jt Surg Am Vol* 1971;53(3):523–37.
- [45] Karami P, Wyss CS, Khoushabi A, Schmocker A, Broome M, Moser C, Pioletti DP. Composite double-network hydrogels to improve adhesion on biological surfaces. *ACS Appl Mater Interfaces* 2018;10(45):38692–9.
- [46] Song W, Ma Z, Wang X, Wang Y, Wu D, Wang C, He Y. Macroporous granular hydrogels functionalized with aligned architecture and small extracellular vesicles stimulate osteoporotic tendon-to-bone healing. *Adv Sci* 2023;10(34):e2304090.
- [47] Ding G, Du J, Hu X, Ao Y. Mesenchymal stem cells from different sources in meniscus repair and regeneration. *Front Bioeng Biotechnol* 2022;10:796367.
- [48] Lu L, Wang J, Fan A, Wang P, Chen R, Lu L, Yin F. Synovial mesenchymal stem cell-derived extracellular vesicles containing microRN555A-26a-5p ameliorate cartilage damage of osteoarthritis. *J Gene Med* 2021;23(11):e3379.
- [49] Li Y, Chen M, Zhou W, Gao S, Luo X, Peng L, Guo Q. Cell-free 3D wet-electrospun PCL/silk fibroin/Sr(2+) scaffold promotes successful total meniscus regeneration in a rabbit model. *Acta Biomater* 2020;113:196–209.
- [50] McNulty AL, Moutos FT, Weinberg JB, Guilak F. Enhanced integrative repair of the porcine meniscus in vitro by inhibition of interleukin-1 or tumor necrosis factor alpha. *Arthritis Rheum* 2007;56(9):3033–42.
- [51] Feng Y, Xiao K, Chen J, Lin J, He Y, He X, Fu Q. Immune-microenvironment modulatory polyurethane-hyaluronic acid hybrid hydrogel scaffolds for diabetic wound treatment. *Carbohydr Polym* 2023;320:121238.
- [52] Yang J, Zhang X, Lu B, Mei J, Xu L, Zhang X, Zhu W. Inflammation-responsive hydrogel spray for synergistic prevention of traumatic heterotopic ossification via dual-homeostatic modulation strategy. *Adv Sci* 2023;10(30):e2302905.
- [53] Khan A, Miller WR, Arias CA. Mechanisms of antimicrobial resistance among hospital-associated pathogens. *Expert Rev Anti Infect Ther* 2018;16(4):269–87.
- [54] Huang M, Ye K, Hu T, Liu K, You M, Wang L, Qin H. Silver nanoparticles attenuate the antimicrobial activity of the innate immune system by inhibiting neutrophil-mediated phagocytosis and reactive oxygen species production. *Int J Nanomed* 2021;16:1345–60.
- [55] Zhong C, Wu Y, Lin H, Liu R. Advances in the antimicrobial treatment of osteomyelitis. *Compos B Eng* 2023;249:110428.